DREVON, Charles
Class of 2023
Academic year 2022–2023

Diplôme d'ingénieur Télécom Physique Strasbourg
3^{rd} year internship report

Characterisation of an accordion lattice setup for a low-dimensional dipolar quantum gases experiment

20/02/2023 – 28/07/2023

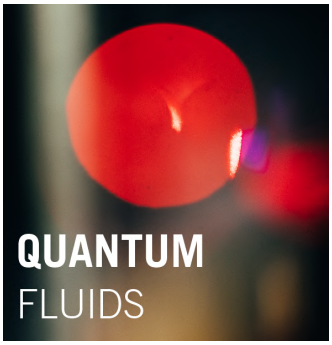

Jun.-Prof. Dr. Lauriane Chomaz
Mail : chomaz@physi.uni-heidelberg.de

Quantum Fluids group
Physikalisches Institut,
Im Neuenheimer Feld 226,
69120 Heidelberg, Germany

Acknowledgements

I would first like to thank Prof. Dr. Lauriane Chomaz for her precious supervision throughout these five months, as well as for giving me the opportunity to carry out an internship in her group. I feel particularly privileged to have been given this chance to work on one of the currently most promising experiments in the field of quantum gases, and I am very grateful to her for making it possible. I am convinced that her and the DyLab team will achieve tremendous contributions to the investigation of dipolar physics, and I will be very happy to follow their progress from wherever I will be in the future. Additionally, I would also like to thank Prof. Dr. Chomaz for her kind support at the beginning of my stay in Heidelberg, when it turned out to be particularly difficult to find accommodation, and when she did everything she could to help me and other interns at the Physikalisches Institut experiencing the same problem to find a solution.

I would then like to thank Valentina Salazar Silva, the Master student who built the accordion lattice setup discussed in this report. She did an amazing job introducing me to the setup, explaining me all the subtleties of her work even though she could not allow me a lot of time as she had to finish to write her thesis at the same time. I am very impressed by the work she has been able to carry out for her Master's thesis, and it was really an honour to take it over. I will keep an excellent memory of the alignment of the accordion lattice in your company Valentina, and I will definitely remember all the songs you used to hum as you were performing it to teach me. I wish you all the best for your PhD in Prof. Dr. Weidemüller's group !

I would also like to thank Dr. Shuwei Jin for introducing me thoroughly to the proper way to conduct lab tasks on a quantum experiment. Benefiting from his wide and precious experience in the field was truly a chance, and I undoubtedly owe him a great deal on a technical level.

I would now like to thank all the other members of the Quantum Fluids group. The PhD students, Karthik Chandrashekara and Jianshun Gao, who contributed to the supervision of this internship and who provided me unconditional support all along it. Thank you Karthik for the fulfilling discussions about music and for sharing your knowledge about the quantum gases community, and thank you Jianshun for all the technical explanations about the lab and for your care daily ! The Master students, Sarah Philips and Thibault Bourgeois, with whom I shared the prep-lab during these five months, as well as the HiWi student Christian Gölzhäuser and the Bachelor students Maurice Rieger and Britta Bader. Finally, the HiWi student Joschka Schöner and the postdoc Wyatt Kirkby, that (re)joined the group when I was finishing this internship. Thank you to all of you for your enjoyable company, it was really a pleasure to work with you ! Thank you also to those of you who made Thibault and I's

lives easier on a day-to-day basis by lending us your Uni cards at the Mensa for lunch - in particular you Jianshun, who provided us that service most of the days !

I would also like to thank Mr. Andreas Düll and the people in the mechanical workshop for the exceptional work they do manufacturing the mechanical parts, as well as the secretary of the group Mrs. Claudia Krämer for the administrative work.

I would then like to thank my friends from France. My friend Amar Bellahsene, from the University of Strasbourg, who performed his Master internship in Heidelberg in Prof. Dr. Weidemüller's group. Life there without you would have been much duller and animated outside work. I wish you all the best for your PhD in Strasbourg at CESQ now ! My friends Mathis Blais, Arthur Dedieu and Alexis Haquet (aka the TDM committee), from Télécom Physique Strasbourg, who followed with attention my journey in Germany, and with whom I continued to spend so many hilarious moments remotely. You guys are really awesome and your friendship is something very precious that I value a lot !

Thank you also to all the other people I met in Heidelberg and that contributed to make of my stay there a very pleasant experience. Thanks then David Feiz, Guo-Xian Su, Eleonora Lippi, Nicolò Antolini, my roommates at Montpellier Haus Clarisse Fournillon, Hibatullah Mimouni, Tany Untoja and Antonia Wilmot-Hall, Julia, Caro, Dillen Lee, Emilie, Esther and Christian.

Furthermore, I would like to thank former Télécom Physique Strasbourg's student Britton Hofer for the inspiration in daring to pursue studies within the field of quantum gases, as well as my teachers Prof. Dr. Anne-Sophie Cordan and Dr. Yann Leroy for their support during my 2nd year at TPS in my ambition to join the Condensed Matter and Nanophysics Master of the University of Strasbourg. I would not be where I am without them.

Finally, I would like to thank my parents for their unconditional support and their availability for me whatever the reason, as well as for their trust in my professional project. This internship would simply not have been possible without them.

Contents

List of Figures

Introduction

Since the first experimental realization of Bose-Einstein condensates (BEC) in 1995 [1, 2], quantum gases have rapidly become a paradigmatic platform for the investigation of many-body quantum phenomena [3], enabling simulation of otherwise inaccessible condensed matter physics problems, and paving the way towards the experimental study of exotic quantum phases of matter. Although for many years most of the quantum gases experiments were dealing with alkali atoms like rubidium or sodium, the last decade marked a turning point on the physical point of view with the achievement of Bose-Einstein condensates of lanthanide atoms. Condensation of dysprosium in 2011 [4] and erbium in 2012 [5] broadened more than ever physicists' perspectives in the study of quantum phase transitions.

These new experiments, taking advantage of the large magnetic moment of lanthanides (approx. $10\mu_B$ for dysprosium - where μ_B is the Bohr magneton - that is to say roughly 10 times the one of an alkaline [6]), expanded considerably the range of experimentally accessible physics problems. Adding long-range and anisotropic interactions to the already exploited short-range interactions of alkali atoms, dipolar quantum gases like Bose-Einstein condensates of dysprosium have indeed proved themselves to constitute excellent systems for the observation of the emergence of new quantum phases, such as quantum droplets or the long-sought supersolid phase. Furthermore, the combination of magnetic atoms and optical lattices - the latter mimicking the crystalline structure of solids with periodically distributed light traps - has also proved being decisive in the experimental study of strongly correlated systems [7, 8].

One of the most exciting and intriguing phenomena occurring in dipolar quantum gases is the emergence of a supersolid phase. Originally mainly discussed in the context of the study of ^{4}He, this counter-intuitive phase exhibits both solid-like and superfluid-like characteristics. Until the achievements of the first dipolar quantum gases experiments, this exotic phase of matter was still very difficult to study experimentally. Its groundbreaking observation in Bose-Einstein condensates of dysprosium and erbium in 2019 [9–11] thus opened a very interesting path towards the investigation of the physics underlying supersolidity. In light of all these reasons, one can easily understand why the implementation of dipolar quantum gases experiments plays a decisive role in contemporary Atomic, Molecular, and Optical physics (AMO).

It is in this context that the internship discussed in this report took place. Performed in Prof. Dr. Lauriane Chomaz's Quantum Fluids group at the Physikalisches Institut of Heidelberg in Germany, this fundamental physics internship aimed at contributing to a cold atom experiment of dysprosium designed to study the physical properties of dipolar quantum gases in reduced dimensions and the phenomena occurring in such physical systems. More

precisely, this experiment aims at investigating phase transitions between the superfluid phase, quantum droplets, and the supersolid phase, as well as the dynamic phenomena taking place in low-dimensional quantum systems.

This experiment, currently under construction in the Quantum Fluids laboratory, involves the creation and study of a quantum gas of ^{164}Dy bosonic dysprosium atoms brought into the phase of a Bose-Einstein condensate and reduced to two dimensions. It involves setting up a system for cooling atoms below the critical temperature of the phase transition between a thermal gas and a Bose-Einstein condensate, as well as a system for tightly confining this condensate in one dimension by compression within a 1D accordion lattice. It is precisely on the implementation of such an accordion lattice for cold atom experiments that this internship is centred on.

Outline

Chapter 1 The first chapter of this report will present the physics institute and the group in which this internship took place.

Chapter 2 The second chapter presents the research field to which the experiment belongs: quantum gases and ultra-cold atoms. The context in which this very active field of contemporary physics was born in the 1990's is briefly recalled, as well as the motivations behind the recent emergence of dipolar quantum gases experiments.

Chapter 3 The third chapter will introduce the main experiment of the group, a dysprosium experiment for the study of low-dimensional dipolar quantum gases, as well as the accordion lattice test setup used during this internship. It will explain briefly the latter setup and the derivation of the expression of the optical potential that this system generates.

Chapter 4 The fourth and last chapter will present the work achieved during this internship, that is to say mainly stability tests undertaken to characterize the accordion lattice setup, and the implementation of a piezoelectric transducer in order to control the optical path difference between interfering beams and thus correct the position of the fringe that will be used to load the atoms.

Presentation of the Physics Institute and the Quantum Fluids group

1

1.1 A brief history of physics in Heidelberg

The history of physics in Heidelberg dates back to the 14^{th} century. Since the first physics lecture in 1387, the University of Heidelberg has become one of the world's most prestigious institutions for physics in the world. No fewer than twenty Nobel Prize of Physics Laureates share a connection with the University of Heidelberg, and many important scientific discoveries and breakthroughs were made in the city [12].

Among other things, Heidelberg is well-known for being the city where German physicist Gustav Kirchhoff, together with his colleague Robert Bunsen, discovered spectra and developed the techniques of spectral analysis in the 1860's, paving the way to our current understanding of the structure of atoms. This outstanding discovery eventually led to the emergence of the field of Atomic, Molecular and Optical physics (AMO) - to which the experiment discussed in this report belongs -, a currently very active field of physics to which Gustav Kirchhoff additionally contributed during his time by defining the concept of a black body [13] and by analysing the spectrum of the sun [14]. The legacy of this pioneering scientist of the 19th century, along with those of his contemporary fellows of the University of Heidelberg such as Hermann von Helmholtz and Robert Bunsen, played a major role in making the city of Heidelberg one of the world's most innovative and dynamic places to conduct academic research in physics.

Nowadays, the academic research in physics carried out in Heidelberg is distributed within different institutes and the internship this report is about was then carried out at the Physikalisches Institut, within the Quantum Fluids group of Prof. Dr. Lauriane Chomaz.

1.2 The Physikalisches Institut

The Physikalisches Institut of Heidelberg is a fundamental physics research organization located in the city of Heidelberg, Baden-Württemberg, Germany (Figure 1.1). It hosts more than 250 people, including researchers, postdoctoral students, PhD students, and Master and Bachelor students.

It is specialized in the experimental investigation of the structure of matter and the fundamental forces, and it is part of the Faculty of Physics and Astronomy of the University of Heidelberg, the oldest University of Germany, founded in 1386.

Figure 1.1: Physikalisches Institut, Im Neuenheimer Feld building 226, Heidelberg, Germany.

The activities of the Physikalisches Institut of Heidelberg cover mainly three specific fields of contemporary physics, namely Low and High Energy Particle Physics, Complex Quantum Systems, and Heavy Ion Physics. These activities are currently organized within several experimental groups, among which figures the group in which the internship took place : the Quantum Fluids group.

1.3 The Quantum Fluids group

The Quantum Fluids group is an experimental physics group created by Prof. Dr. Lauriane Chomaz in February 2021, and aiming to study low-dimensional dipolar quantum physics using ultra-cold atoms of dysprosium of bosonic isotope ^{164}Dy. During the internship, in addition to the principal investigator Prof. Dr. Chomaz, the group was composed of one postdoctoral researcher (Dr. Shuwei Jin), two PhD students (Karthik Chandrashekara and Jianshun Gao), one Master student (Sarah Philips), two Master interns (Thibault Bourgeois and me), one HiWi student (Christian Gölzhäuser), and two Bachelor students (Maurice Rieger and Britta Bader). Moreover, at the very beginning of my stay, another Master student (Valentina Salazar Silva) was also part of the team, finishing writing her Master's thesis, and at the very end of it, one additional postdoctoral researcher (Dr. Wyatt Kirkby) and one additional HiWi student (Joschka Schöner) (re)joined the group.

1.3.1 Organisation of work

Within the group, work is organised on the basis of flexible working hours, generally from 9.30am to 7pm, and includes a weekly meeting of approximately one hour and a half on Tuesday mornings at 10am. Besides from the laboratory, the group has two shared spaces for students and two personal offices for the group leader and postdoctoral fellow. The laboratory

(a) Main Lab. **(b)** Prep Lab.

Figure 1.2: The Quantum Fluids group laboratory.

consists of two rooms directly connected to each other (Figure 1.2), one hosting the main experiment and the other one used to build the test setups to implement in the future on the main experiment.

1.3.2 Activities of the group

The experiment being in construction, most of the work carried out by the team during my stay have been consisting in building the main setup regarding the postdoctoral researcher and the PhD students, and in building the test setups regarding the Master student and interns. To set the scene, at the time of the internship, the main experiment already included all the parts required to achieve three-dimensional Bose-Einstein condensates of dysprosium - which was actually accomplished by the team in April, 2023 - but not yet the full imaging system, the accordion lattice setup (the system designed to reach the two-dimensional regime), and the Digital Micro-mirror Device (DMD) setup (the system aimed at dynamically configuring the trapping potential experienced by the atoms). Those three previous systems were respectively the subjects of the work of Sarah, Valentina and I, and Thibault.

Towards quasi-two-dimensional dipolar quantum gases of Dy

2

2.1 Quantum gases

2.1.1 The early years : towards absolute zero

Quantum gases have been the subject of intense experimental research in physics for almost 30 years now [1, 2], and even longer if we take into account preliminary work undertaken as early as the 1980s [15, 16]. To better understand the emergence of this field of research, we need to go back to the beginning of the 20th century, when a group of physicists were relentlessly engaged in a frantic race to the conquest of absolute zero temperature, aiming in particular at the liquefaction of the last atmospheric gas ever to be liquefied: helium. This achievement, finally realized in 1908, led physicists to the fascinating discovery of new, hitherto unknown phases of matter: the superconducting phase in 1911 and the superfluid phase in 1937. The experimental observation of these impressive manifestations of quantum theory on the macroscopic scale provided even greater motivation for physicists to investigate the properties of matter at low temperatures, and the theoretical prediction of another macroscopic quantum phenomenon, Bose-Einstein condensation, in 1924-1925, further strengthened their interest by defining a new experimental objective. In order to provide a context for the work reported in this report, these events are briefly introduced here from a historical point of view. A more detailed introduction can be found in references [17–19].

The conquest of absolute cold

At the beginning of the 20th century, Europe was in a relentless race to reach absolute zero temperature. The ground-breaking experiments and fascinating discoveries that accompanied this race gave rise to various fields of research in contemporary physics, including that of cold atoms.

On June 10, 1908, after 10 years of dedicated work, Dutch physicist Heike Kamerlingh Onnes (a former student of Bunsen and Kirchhoff at the University of Heidelberg) succeeded in liquefying helium-4 in his laboratory at the University of Leiden in the Netherlands, achieving the lowest temperatures of the time ($T < 4.2$K) [20]. Three years later, in 1911, while he was continuing his research work on the properties of matter at low temperatures, Onnes discovered a new phase of matter within a sample of mercury [21] : the superconducting phase, an intriguing phase characterized by a total absence of electrical resistance and the complete expulsion of all magnetic fields (the Meissner-Ochsenfeld effect). "For his investigations on

the properties of matter at low temperatures which led, inter alia, to the production of liquid helium", Onnes will received in 1913 the Nobel Prize in Physics.

A few years later, in 1937, the superfluid phase was discovered. This second new phase, observed in helium-4 independently by Pyotr Kapitsa [22] at the Russian Academy of Sciences and by John F. Allen and Don Misener [23] at the University of Cambridge in England, is characterized by zero viscosity, resulting in the undissipated flow of its constituents. It would later become clear that the phenomenon of superconductivity - akin to the superfluidity of conduction electrons in a metal - and the phenomenon of superfluidity are not unrelated to a third macroscopic phenomenon of quantum origin: Bose-Einstein condensation.

The theoretical prediction of Bose-Einstein condensation

In 1924, the young Indian theoretical physicist Satyendra Nath Bose succeeded in deriving the law describing the spectrum of radiation emitted by a black body (Planck's law) by means of a statistical argument, treating radiation as a gas of identical particles. He then sent a letter to Albert Einstein, with a copy of his article, which aroused Einstein's interest, who then translated it from English into German and published it [24]. Shortly afterwards, Einstein generalized this approach to the study of a perfect gas of identical material particles in two articles in 1924 [25] and 1925 [26], and succeeded in establishing the expression for the energy distribution of a monoatomic perfect gas: the Bose-Einstein distribution.

Bose-Einstein distribution

Let's consider a set of identical atoms, with no mutual interactions, in contact with a thermostat. The objective is to find the most probable macroscopic state of the gas for fixed values of the total number N of atoms and the average total energy E of these atoms. To do this, the number of distinct microscopic states associated with a macroscopic state of the gas is defined as the number N_i of atoms in each energy range Ei to $Ei + \Delta E_i$.

One can then write :

$$\sum_i N_i = N \quad \sum_i N_i E_i = E \tag{2.1}$$

And it can be shown that the average occupation number n_i of a quantum state i of energy E_i is given by :

$$n_i = \frac{1}{\exp\left[\beta\left(E_i - \mu\right)\right] - 1} \tag{2.2}$$

which is the Bose-Einstein distribution.

In this expression, β and μ are constants ("Lagrange multipliers") derived from the constraints 2.1. The first constant, β, is related to the temperature T of the thermostat by the equation $\beta = \frac{1}{k_B T}$, where k_B is Boltzmann's constant; the second, μ, is the chemical potential, i.e. the energy required to add an atom to the gas.

The formulas established by Einstein in his second article led him to predict a curious effect. If, for a fixed volume V and total number N of atoms, the temperature T of the gas is reduced, it is found that below a certain critical temperature T_C the atoms must accumulate in the ground state of the box containing the atoms. This state thus acquires a macroscopic population, which can become of the order of N as the temperature is further reduced: this is the phenomenon of Bose-Einstein condensation.

However, the low temperatures predicted by Einstein's calculations, far below the usual temperatures expected for a gas, together with experimental inaccessibility, led most physicists of the time to doubt about the real existence of this phenomenon, starting, it seems, with Einstein himself [27]. It was only with the development of laser and evaporation cooling techniques for atoms that the reality of the phenomenon really took hold, when the first experimental observation took place in quantum gases.

It was thus in the footsteps of the pioneering experiments of early 20th-century physicists, and with the Bose-Einstein condensation phenomenon as objective, that the field of research to which the experiment discussed in this report belongs emerged in the 1980s: quantum gases.

2.1.2 The first Bose–Einstein condensates

First attempts with spin-polarized hydrogen atoms

One might wonder why the theoretical prediction of Bose-Einstein condensation did not immediately lead to experimental initiatives to observe it in reality. The reason is quite simple: Einstein's theory predicts a very low phase transition temperature towards Bose-Einstein condensation, too low for a dilute gas to exist in a stable state. Moreover, gaseous substances were always observed to undergo quite ordinary condensation to a liquid phase and then to a solid phase before even approaching this critical temperature, reducing the phenomenon to a purely theoretical concept at first.

Nonetheless, it is indeed in dilute gases that the Bose-Einstein condensates observed in contemporary cold atom experiments are formed. One idea to overcome this difficulty was then to consider metastable gas states with sufficiently long lifetimes to enable precise observations.

In particular, a paper by Stwalley and Nosanov [28] published in 1976, inspired by a 1959 article written by Hecht [29], proposed to polarize the electron spins of atomic hydrogen in

order to block the molecular recombination of atoms and thus stabilize a hydrogen gas at an arbitrarily low temperature. Several experimental physics groups undertook this task in the late 1970s and early 1980s, most notably in Amsterdam, where Isaac F. Silvera and J. T. M. Walraven showed that the realization of such a gas was indeed possible [15], although they unfortunately failed to achieve Bose-Einstein condensation.

Successful experiments with alkali atoms

In parallel with the hydrogen experiments, and independently of them, radically different atom-cooling experiments were carried out with alkaline atoms such as sodium and rubidium. The idea behind these experiments, which was new at the time, was to slow down atoms by interaction with laser light beams, taking advantage of the momentum exchange between light and matter. To achieve this, the main constraint was to have a relatively intense laser source emitting at a frequency close to an atomic resonance frequency. For this reason, physicists' interest shifted from hydrogen atoms, whose resonance frequencies are in the far ultraviolet, to alkaline atoms, whose resonance frequencies are in the visible or infrared range, making them easier to manipulate.

The simplest radiative cooling mechanism, "Doppler cooling", was proposed in 1975 by T. Hänsch and A. Schawlow for neutral atoms [30], and by D. Winelmand and H. Dehmelt for ions [31]. Its principle is based on the so-called "radiation pressure" force exerted by a laser beam on an atom - a force which is nothing other than the mechanical pressure exerted by light on a surface through momentum exchange between the latter and the electromagnetic field. A brief description of Doppler cooling is given here:

Two laser beams of the same frequency and intensity but propagating in opposite directions are shone on the atoms. The frequency of the light waves is chosen to be slightly lower than the resonance frequency of the atoms.

Then consider a stationary atom as shown in Figure 2.1 ; by symmetry, the two radiation pressure forces are of equal intensity and opposite direction, so that they cancel each other out and the atom feels no resultant force.

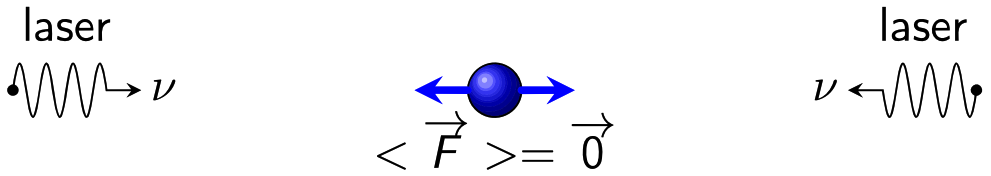

Figure 2.1: A stationary atom : by symmetry, the two radiation pressure forces cancel each other out and the atom feels no resultant force. (taken from Jimmy Roussel [32]).

Now consider an atom in motion like in Figure 2.2 , to the right, for example. Because of the Doppler effect, the atom will "see" the wave coming towards it with an increased

frequency, closer to resonance. The radiation pressure created by this wave will therefore be greater than for an atom at rest. On the other hand, the wave coming from the left, travelling in the same direction as the atom, is seen by the atom with a frequency lower than its actual frequency. The force it generates is therefore less than that acting on a stationary atom. In the end, the balance between the two forces is broken for a moving atom, to the benefit of the laser beam meeting the atom. The resulting force is opposed to the atomic velocity, and therefore corresponds to a frictional force. In this way, atoms can be slowed down, and thus cooled, by interaction with light.

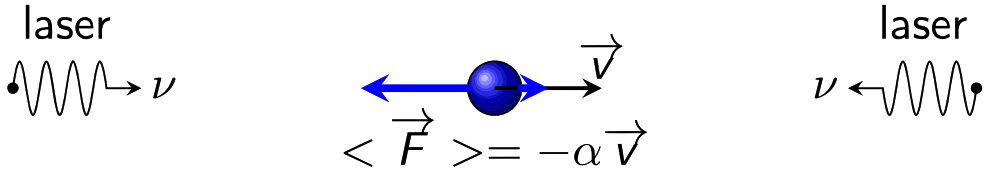

Figure 2.2: An atom in motion : because of the Doppler effect, the balance between the two radiation pressure forces is broken and the resulting force is opposed to the atomic velocity. (taken from Jimmy Roussel [32]).

With this method, temperatures of the order of a hundred microkelvin are reached within a volume of the order of a cubic centimetre. The result is a so-called "optical molasses", as momentum exchanges make the medium viscous to the atoms [16].

Radiative cooling is however not sufficient to reach the phase transition temperature towards the Bose-Einstein condensate. To finally achieve this, a completely different kind of cooling process must follow: evaporative cooling. The principle is quite simple: it consists in cooling the sample by evacuation of the most energetic atoms and thermalisation to a lower temperature - just like when one blows on a hot drink in order to cool it down by evacuating the vapour off its surface. This is usually achieved using a trapping device referred to as a magneto-optical trap (MOT).

By positioning atoms in a non homogeneous magnetic field, an additional force can be generated, this time a trapping force, which tends to accumulate the atoms where the magnetic field cancels out. In such a trap, each atom couples to the local magnetic field $\vec{B}$ by interacting with its magnetic moment $\vec{\mu}$, giving rise to the interaction energy $E = -\vec{\mu} \cdot \vec{B}$. By realizing a local minimum of the magnetic field $\vec{\mu}$ and orienting the magnetic moment $\vec{\mu}$ of the atoms in the opposite direction to the magnetic field, the interaction energy then simply becomes $E = |\vec{\mu}||\vec{B}|$. This energy, which acts as a potential energy for the movement of the atoms' center of mass, is then minimal at the same point as $|\vec{B}|$. In this way, the atoms are forced to remain confined to the potential well constituted by the magnetic field minimum, in order to minimize the interaction energy.

To evaporate the atoms, the height of the potential well is varied, starting from a high depth that is gradually lowered (see Figure 2.3). It was by taking advantage of this technique

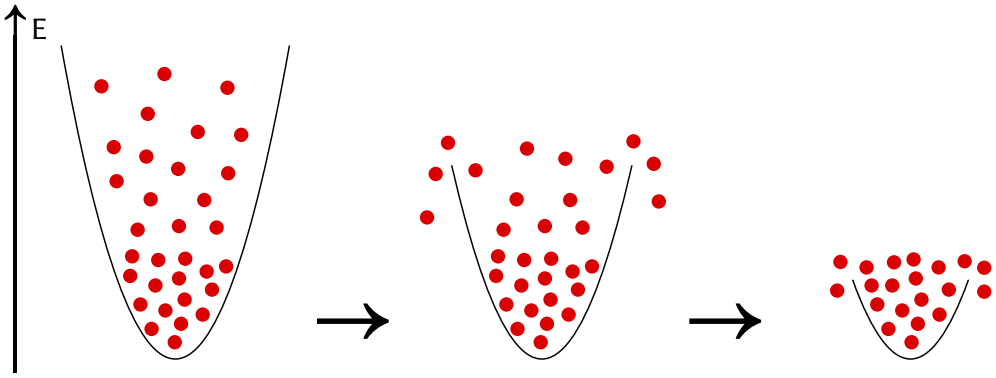

Figure 2.3: To evaporate the atoms, the height of the potential well is varied, starting from a high depth that is gradually lowered.

that the first experimental observations of atomic Bose-Einstein condensates were made in 1995. First at Boulder, in the group of E. Cornell and C. Wieman with rubidium atoms [1], then at MIT in W. Ketterle's team with sodium atoms [2]. "For the achievement of Bose-Einstein condensation in dilute gases of alkali atoms, and for early fundamental studies of the properties of the condensate", Cornell, Wieman and Ketterle were awarded the Nobel Prize in Physics in 2001.

2.2 Dipolar quantum gases

2.2.1 Lanthanide atoms

Magnetic atoms for new experiments with large magnetic moments

In quantum gases, properties are controlled by interparticle interactions. In an effort to produce even more intriguing properties, the realization of quantum gases with different interactions has thus been highly sought-after, leading researchers to notice that the dipolar interaction acting between particles with a permanent dipole moment (such as a magnetic moment) should result in new phenomena [33].

Following the first Bose-Einstein condensation experiments (carried out using rubidium and sodium, so alkali atoms), most of the ultra-cold atoms experiments undertaken until the early 2010's involved alkalis, which are species that have negligible magnetic dipole moments. The achievement of Bose-Einstein condensates of lanthanide atoms such as dysprosium in 2011 [4] and erbium in 2012 [5], species with a large magnetic dipole moment, marked a turning point in the research field of quantum gases, leading to the emergence of a new branch of cold atoms : dipolar quantum gases.

Dysprosium atoms : a promising platform for dipolar quantum physics

It is in this context that ultra-cold atom experiments using dysprosium atoms have appeared in recent years, taking advantage of the large magnetic dipole moment of this lanthanide : $\mu_{Dy} \approx 10\mu_B$, where μ_B is the Bohr magneton (that is to say roughly 10 times the one of an alkaline [6]).

2.2.2 Interparticle interactions

Contact interaction

In the reference frame of the centre of mass of a 2-particle system, the real interatomic potential is the usual van der Waals interaction (see Figure 2.4). At long distances, this interaction decreases as $1/r^6$, with r the distance between the particles. It can therefore be replaced by a short-range and isotropic pseudo-potential : the so-called "contact" interaction [34].

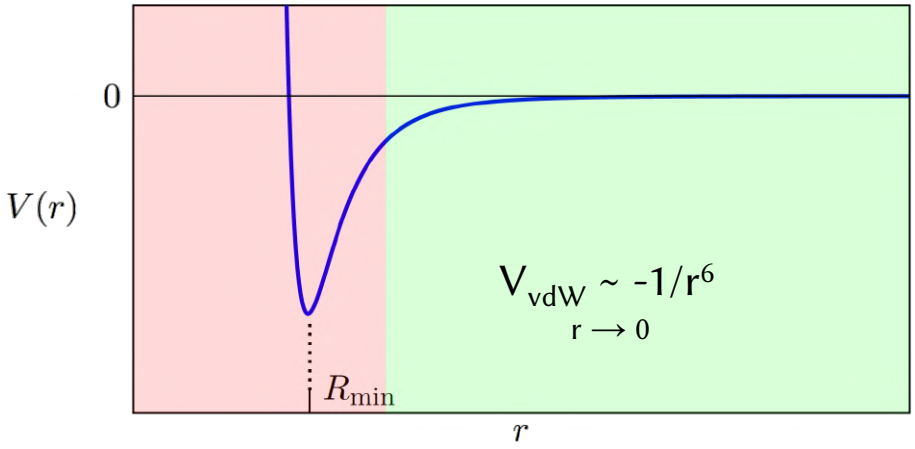

Figure 2.4: At long distances, the van der Waals interaction decreases as $1/r^6$, with r the distance between the particles (adapted from Jean Dalibard [34]).

In the regime of temperature that is characteristic of quantum gases experiments (that is to say for temperature belonging to the nK range), only s-wave scattering between particles generally occur. In these conditions, the s-wave scattering length a is the quantity characterising this "contact" interaction, which then reads :

$$U_{contact}(\vec{r}) = \frac{4\pi\hbar^2 a}{m}\delta(\vec{r}) \equiv g\delta(\vec{r}), \tag{2.3}$$

with m the mass of an atom, and $g = \frac{4\pi\hbar^2 a}{m}$ the amplitude of the contact interaction.

This contact interaction is then short-range and isotropic.

Dipolar interaction

As mentioned at the beginning of the chapter, dipolar interaction is the additional ingredient in dipolar quantum gases in comparison with quantum gases of alkali atoms. In such systems, dipolar interaction comes from the magnetic interaction occurring between two atoms via their magnetic dipole moment. This interaction is very different from the contact interaction and thus results in new phenomena.

Let's consider two particles labelled A and B with dipole moments $\vec{D_A}$ and $\vec{D_B}$ and whose relative position is $\vec{r} = r\vec{u}$ like in Figure 2.5.

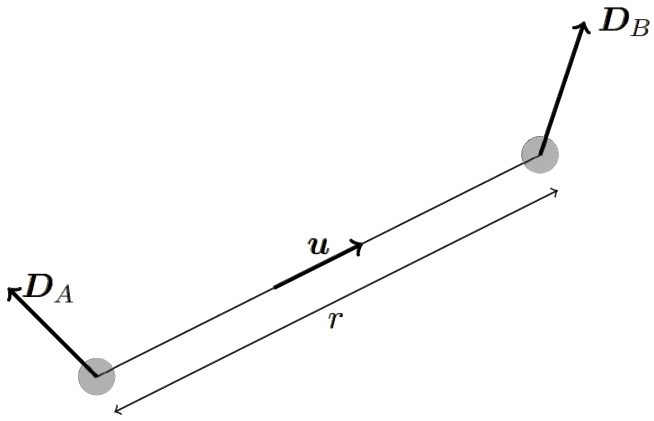

Figure 2.5: Two particles with dipole moments $\vec{D_A}$ and $\vec{D_B}$ and with relative position $\vec{r} = r\vec{u}$ (taken from Jean Dalibard [34]).

The interaction energy reads :

$$U_{\text{dip}} = \frac{\mu_0 \mu^2}{4\pi r^3} \left[\vec{D}_A \cdot \vec{D}_B - 3 \left(\vec{u} \cdot \vec{D}_A \right) \left(\vec{u} \cdot \vec{D}_B \right) \right] \tag{2.4}$$

with μ the magnetic dipole moment and μ_0 the permeability of vacuum.

Let's consider the polarized configuration for which both dipoles point in the same direction as in Figure 2.6.

The energy then reads :

$$U_{dd}(\vec{r}) = \frac{\mu_0 \mu^2}{4\pi} \frac{1 - 3\cos^2 \theta}{r^3}, \tag{2.5}$$

where θ is the angle between the direction of polarization and the direction joining both particles.

It is then obvious that dipolar interaction is very different from contact interaction as it is long-range because of its decay in $1/r^3$, and anisotropic because of its dependence on θ.

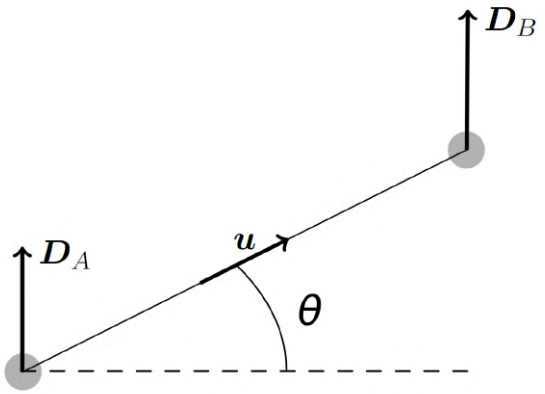

Figure 2.6: The polarized configuration : both dipoles point in the same direction (adapted from Jean Dalibard [34]).

Furthermore, when θ varies between 0 and $\pi/2$, the factor $1 - 3\cos^2\theta$ varies between -2 and 1. This means that the dipolar interaction is repulsive for particles sitting side by side but attractive for dipoles sitting on top of each other (the so-called 'head-to-tail' configuration).

In order to compare the strength of this interaction with the one of the contact interaction, it is then interesting to define a characteristic length, the so-called 'dipolar length' :

$$a_{dd} \equiv \frac{\mu_0 \mu^2 m}{12\pi\hbar^2}. \tag{2.6}$$

It is then convenient to define the so-called "dipolar parameter" ϵ_{dd}, i.e. the ratio between the dipolar length characteristic of dipolar interaction and the s-wave scattering length characteristic of contact interaction [7] :

$$\epsilon_{dd} \equiv \frac{a_{dd}}{a} = \frac{\mu_0 \mu^2}{3g} \tag{2.7}$$

To observe dipolar effects, this dipolar parameter therefore needs to be non negligible.

Feshbach resonances, a tool to tune interactions

From an experimental point of view, the scattering length a can be tuned using an external magnetic field via the so-called Feshbach resonance phenomena [35, 36], which is low energy scattering resonance occurring between two scattering channels when two particles collide (one closed channel of low energy and one open channel of higher energy).

Close to a Feschbach resonance, the scattering length a indeed varies with the external magnetic field B as :

$$a = a_{bg}\left(1 - \frac{\Delta}{B - B_0}\right), \tag{2.8}$$

where a_{bg} is the so-called "background scattering length", B_0 is magnetic field value for which the resonance is reached, and Δ is the width of the resonance. It is then interesting to use Feschbach resonances decrease as much as possible the scattering length so that ϵ_{dd} gets bigger and thus dipolar effects important.

2.2.3 New exotic states of matter

Dipolar interactions in quantum gases result in new exotic phenomena. In particular, a so-called "quantum droplet" state and the long-sought supersolid phase have already been successfully observed in such systems. The combination of dipolar interactions and low dimensions is therefore expected to give rise to exotic configurations with a high degree of controllability, probably even more than in the experiments carried out with non-dipolar quantum gases. This is the fundamental motivation behind the experiment undertaken by the Quantum Fluids group.

Quantum droplets

As previously explained, the dipolar interaction is long-range and anisotropic, and it is precisely for those reasons that new phenomena occur. Actually, it was already known in the context of classical fluids that long-range and/or anisotropic interactions give rise to new phenomena [33]. In particular, in a ferrofluid - that is to say in a liquid presenting ferromagnetic subdomains of typical dimensions of 10nm - an instability can occur thanks to these properties when a magnetic field is perpendicularly applied to its surface : the Rosensweig instability (Figure 2.7).

Figure 2.7: The Rosensweig instability in a ferrofluid (taken from Holger Knieling et. al [37]).

One interesting phenomenon occurring in dipolar quantum gases is the emergence of the quantum version of the aforementioned Rosensweig instability appearing in classical ferrofluids : the so-called quantum droplets.

Indeed, as it can easily be understood with 2.5, as the most favourable configuration is the one for which the energy is minimized, a dipolar quantum gas evolving in free space will therefore tend to the configuration where all the dipoles seat on top of each other. If the atoms are trapped into an optical potential, the favourited configuration cannot be a very long one dimensional chain of dipoles and the system then breaks up into several one dimensional pieces, forming so-called "quantum droplets", as depicted in Figure 2.8.

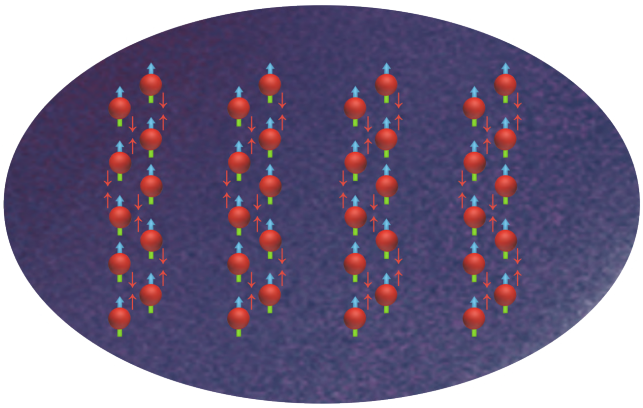

Figure 2.8: Quantum droplets : the dipoles seat on top of each other resulting in several one dimensional pieces.

Supersolidity

Another intriguing phenomena occurring in dipolar quantum gases is the apparition of a supersolid phase. Originally mainly discussed in the context of the study of ^{4}He [38], this counter-intuitive phase exhibits characteristics of both a solid and a superfluid, respectively with spatial modulation in density and global phase coherence (see Figure 2.9).

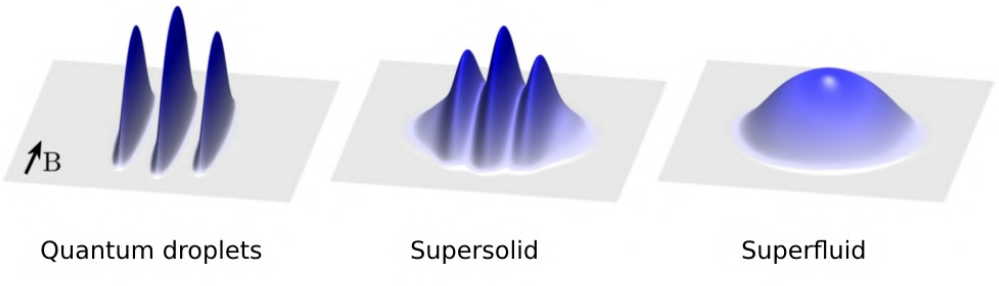

Figure 2.9: Exotic phases of matter : on the left, quantum droplets ; in the centre, supersolidity ; and on the right, superfluidity (adapted from Fabian Böttcher [39]).

Until the achievements of the first dipolar quantum gases experiments, this exotic phase of matter was still very difficult to study experimentally. Its groundbreaking observation in Bose-Einstein condensates of dysprosium and erbium in 2019 [9–11] thus opened a very interesting path towards the investigation of the physics underlying this phenomena.

A supersolid is formerly a quantum system that spontaneously breaks both translational invariance and U(1) gauge symmetry. In the simplest case, which was the one first brought on by Eugene Gross more than 50 years ago [40], a supersolid can be seen as a system which has a macroscopic wavefunction ψ with a well defined phase ϕ as in a superfluid but with a periodic modulation of the density as in a solid [41] - or also, equivalently, as a coherent crystal, that is to say a solid like structure whose nodes are mutually coherent together.

BKT phase transition as a perspective

Finally, the experiment of the Quantum Fluids group aims to study quasi-two-dimensional systems. This is motivated by the very different mechanism occuring in that configuration, starting with the so-called Berezinskii–Kosterlitz–Thouless (BKT) transition, which is a topological phase transition that does not exhibit any spontaneous symmetry breaking.

In particular, the BKT transition is a phase transition occurring in the two-dimensional XY model, a lattice model of magnetic moments (or spins) where each spin interacts with its neighbours via an exchange interaction [42].

In three dimensions, below a critical temperature, the spins spontaneously order themselves in the same direction. The system is then in a so-called ferromagnetic phase characterised by a non-zero total magnetisation where the rotational symmetry of all the magnetic moments is broken by the anisotropy of the direction of the magnetisation.

In two dimensions, however, it has been shown that a continuous symmetry such as that of the XY model cannot be spontaneously broken and that no ferromagnetic-paramagnetic phase transition can therefore take place. Nevertheless, Vadim Berezinsky in 1972 and independently John M. Kosterlitz and David J. Thouless in 1973 showed that a phase transition did in fact take place, but that this transition was of a purely topological nature: this is the BKT transition. "For theoretical discoveries of topological phase transitions and topological phases of matter", Thouless and Kosterlitz were awarded the Nobel Prize in Physics 2016.

Introduction to the experimental setup 3

3.1 Trapping and cooling of dysprosium atoms

3.1.1 Atomic beam generation and laser cooling

The generation of a Bose-Einstein condensate requires the implementation of a system for producing and cooling atoms [43]. The first step is to generate a thermal gas of dysprosium by heating granules of this species in an high-temperature effusion oven to a temperature of around 1000°C. At the exit of the oven, the gas enters a two-dimensional magneto-optical trap (2D MOT), a system designed to cool and confine the thermal gas in two dimensions, thus producing a slow linear sample of atoms. This sample is then pushed into a second magneto-optical trap, this time three-dimensional (3D MOT), cooling and confining the thermal gas in all three dimensions of space. These magneto-optical traps thus perform laser cooling of the gas (Doppler cooling), slowing down the atoms and confining them to a restricted volume of space. A schematic view of the experimental setup is shown in Figure 3.1. The Quantum Fluids group thus reported in their first paper [44] to have observed efficient loading of the 3D MOT with rates $\phi_{3D} \gtrsim 10^8$ atoms/s and saturation atom numbers of $N_{sat} \approx 3 \times 10^8$ at a moderate oven reservoir temperature of 800°C.

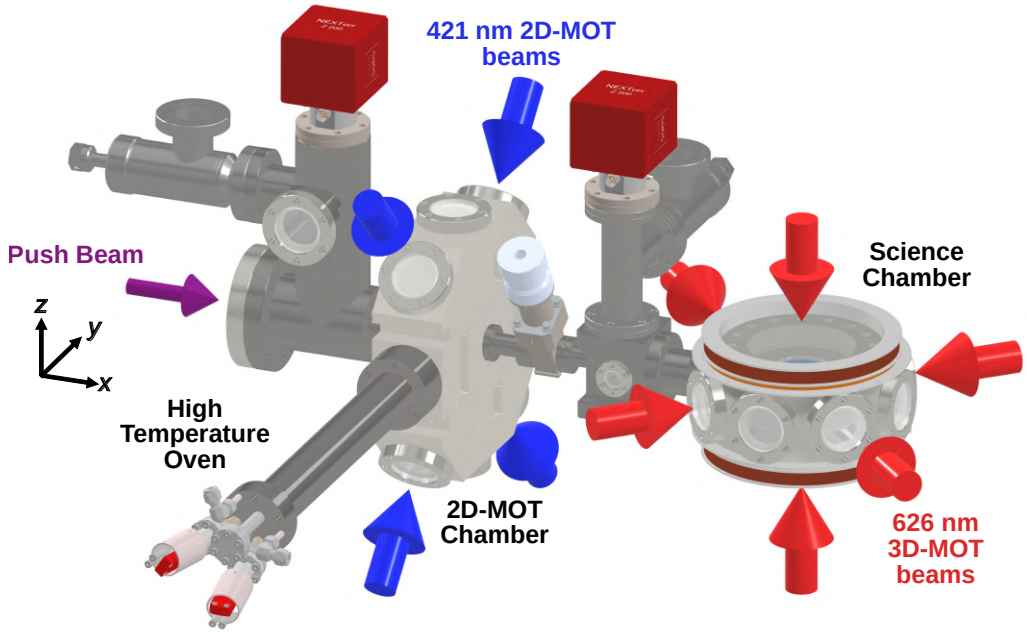

Figure 3.1: Illustration of the atom cooling setup in the Quantum Fluids group experiment in Heidelberg (taken from Shuwei Jin et al. [44]).

3.1.2 Evaporative cooling

This "radiative" cooling is not sufficient to reach the phase of the Bose-Einstein condensate. It is therefore necessary to carry out "evaporative" cooling (2.1.2). This cooling involves not only a decrease in temperature, but also a diminution in the number of atoms in the sample. To achieve this, the gas is loaded into an optical dipole trap (ODT) [45], whose precise handling performs this evaporative cooling and enables to reach the phase of the Bose-Einstein condensate (the Quantum Fluids group achieved its first Bose-Einstein condensate of dysprosium at the time of this internship, in April 2023).

3.2 Two-dimensional compression with an accordion lattice

As the aim of the Quantum Fluids group is to study 2D gases, the following step after reaching quantum degeneracy is to confine the sample very tightly along one dimension by compressing it within an optical accordion lattice [46]. In this section, we expose the main ideas behind such a system. A detailed explanation of the accordion lattice from both a technical and a physical point of view can be found in Valentina Salazar Silva's Master thesis [47].

3.2.1 Working principle and test setup

Working principle

An accordion lattice is a standing wave realizing an optical dipole trap for atoms and whose periodicity can be dynamically configured, enabling to compress a cloud of atoms down to a quasi-two-dimensional geometry. This type of system, first implemented by Li et al. in 2008 [48], has been successfully used in several quantum gases experiments, like for example by Ville et al. in [49]. In such setup, two coherent laser beams meet at the position of the cloud. The two beams interfere resulting in a set of rectilinear interference fringes. Additionally, the fringe-to-fringe distance can be dynamically modified. The idea here is therefore to load the quantum gas into the central fringe of this lattice when it is set so that the fringe spacing is of the order of magnitude of the extent of the three-dimensional condensate, and then to continuously reduce this fringe spacing until it achieves quasi-two-dimensional geometry.

Test setup

To achieve this, a two-level set of optical components was designed and implemented in the test lab by Valentina Salazar Silva. This setup, depicted in Figure 3.2, comprises a lower floor that shapes a laser beam using half-wave plates, a Polarizing Beam Splitter (PBS) and a telescope, as well as a 45° mirror mounted on a linear translation stage that brings the laser beam to an upper floor.

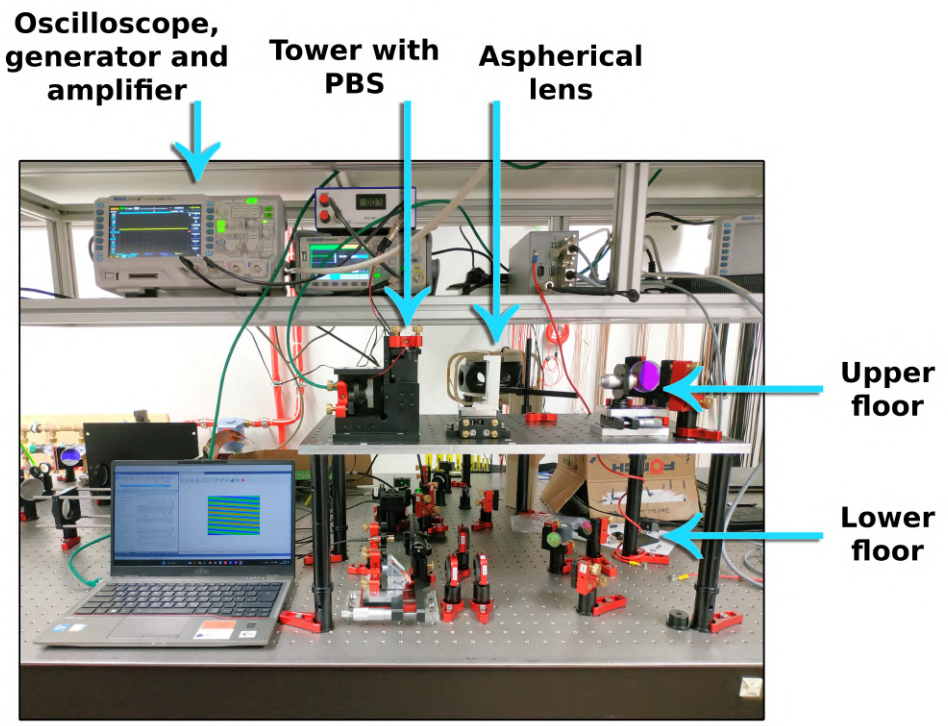

Figure 3.2: The accordion lattice setup in the prep Lab of the Quantum Fluids group.

In the upper floor, the beam is split into two by a second PBS. One of these beams (the lower beam) is then redirected towards the back of the beam splitter, where it meets at the exit a quarter-wave plate and a mirror (the back mirror) enabling it to propagate in the same direction, but in the reverse sense at the opposite exit of the beam splitter. The second beam (the upper beam) encounters a simple 45° mirror at the exit of the beam splitter, redirecting it in the same direction and the same sense as the lower beam. Thus two parallel beams are formed. These two beams then meet an aspherical lens that focuses them at its focal point, and which is mounted on a 4-axis stage allowing its alignment.

The whole challenge of this type of system then lies in the ability to dynamically and continuously vary the distance D separating the two beams at the entrance of the lens, which is achieved by the last component of the lower floor, namely the mirror mounted on a linear translation stage, whose position controls the entrance position of the initial beam into the second beam splitter, and thus the spacing between the two beams at the exit of the latter (see Figure 3.3).

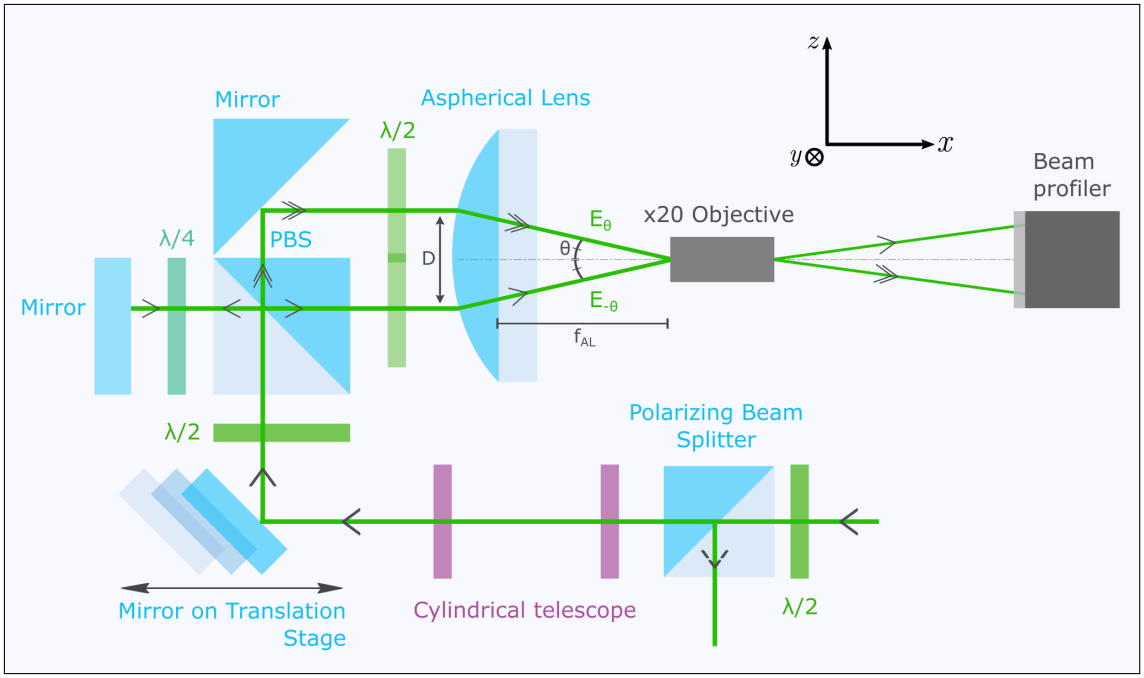

Figure 3.3: Illustration of the accordion lattice test setup (adapted from Valentina Salazar Silva [47]).

3.2.2 Mathematical model of the interference pattern

The interference pattern resulting from an accordion lattice can be analytically calculated. Here are some explanations about it, adapted from [47].

As illustrated in Figure 3.3, the two parallel beams meeting the lens emerge out of it making an angle θ with the optical axis. Calling E_θ and $E_{-\theta}$ respectively the upper and the lower beam, the intensity of the interference pattern is then given by :

$$I_{\text{tot}}(x,y,z) = |E_\theta + E_{-\theta}|^2 \tag{3.1}$$

$$= |E_\theta|^2 + |E_{-\theta}|^2 + E_\theta^* E_{-\theta} + E_\theta E_{-\theta}^* \tag{3.2}$$

Using $E_{\pm\theta} = \sqrt{I_{\pm\theta}}\exp(ik_{\pm\theta}.r + \varphi_{\pm\theta})$, the analytical derivation yields [47] :

$$I_{\text{tot}}(x,y,z) = I_\theta + I_{-\theta} + 2\sqrt{I_\theta}\sqrt{I_{-\theta}} \cdot \cos\left(\frac{4\pi}{\lambda} z \sin(\theta) + \Delta\varphi\right). \tag{3.3}$$

where $\Delta\varphi = \varphi_\theta - \varphi_{-\theta}$ is the beam-to-beam phase shift - also given by $\Delta\varphi = \frac{\delta}{2\pi\lambda}$, with δ the optical path difference and λ the laser wavelength - and $I_{\pm\theta}$ are the individual beams intensities.

One then immediately identifies the expression of the so-called fringe spacing d :

$$d = \frac{\lambda}{2\sin(\theta)} \tag{3.4}$$

which allows I_{tot} to be rewritten :

$$I_{\text{tot}}(x, y, z) = I_\theta + I_{-\theta} + 2\sqrt{I_\theta}\sqrt{I_{-\theta}} \cdot \cos\left(\frac{2\pi}{d}z + \Delta\varphi\right). \tag{3.5}$$

This expression will be used to fit experimental data and extract the beam-to-beam phase shift $\Delta\varphi$.

Furthermore, the fringe spacing d can be written as a simple function of configuration parameters which will be important for characterisations. Indeed, as deduced from Figure 3.3, one can write :

$$\sin(\theta) = \frac{\frac{D}{2}}{\sqrt{\left(\frac{D}{2}\right)^2 + f_{AL}^2}} \tag{3.6}$$

where D is the distance separating the two beams at the entrance of the lens, and f_{AL} the focal length of the lens.

With 3.4, one can then write that, providing excellent alignment of all the optical components, horizontal rectilinear interference fringes are observed at the focal point of the lens with fringe spacing:

$$d = \lambda\sqrt{\frac{1}{4} + \frac{f_{AL}^2}{D^2}} \tag{3.7}$$

3.2.3 Stabilizing the interference pattern

Piezoelectric mounting structure

One of the challenge of such an accordion lattice setup is the stabilization of the interference pattern. Indeed, the optical potential confining the atoms should keep a stable position all along the compression in order for this to be adiabatic, and this position should also be stable in short and long time after the achievement of the compression in order to prevent unwanted shaking or loss of the atoms.

One way to control that position is to use a piezoelectric transducer (PZT, see Figure 3.4) glued at the back of the back mirror to finely tune the optical path length covered by the

lower beam, and therefore the optical path length difference between the two beams at the interference point (or, in other words, the phase shift between the two beams). A massive and custom-shaped brass mounting structure has to be glued to the available face of the piezoelectric transducer. This mounting structure allows passive control over the resonant frequencies of the mechanical system constituted by the back mirror.

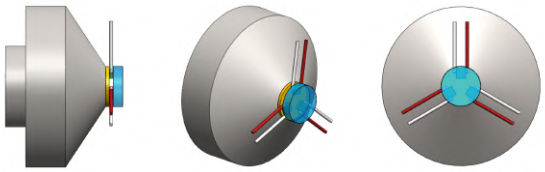

Figure 3.4: 3D model of a piezoelectric actuator mounting structure designed for ultra-cold atoms experiments (taken from Eric Magnan [50]).

Motorized linear stage

Furthermore, to achieve adiabatic compression of the Bose-Einstein condensate on the main experiment, a motorized linear stage for the bottom mirror has to be implemented instead of the manual one already used in the test setup. The choice of this motorized stage was done regarding the importance of magnetism in the experiment, meaning that it should comprise as less magnetic component as possible to avoid unwanted interactions with the atoms. The *V-408 PIMag Linear stage* from Physik Instrumente has thus been chosen and implemented on the test setup (Figure 3.5).

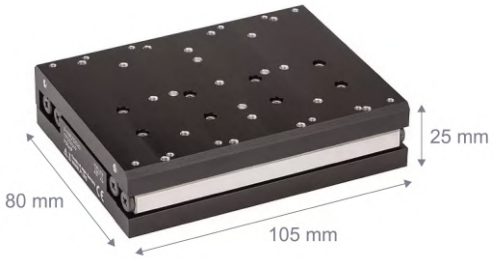

Figure 3.5: Motorized linear stage V-408 PIMag from Physik Instrumente chosen for adiabatic compression of the Bose-Einstein condensate (taken from Valentina Salazar Silva [47]).

Characterization of the accordion lattice 4

4.1 Chronological review of the work achieved

In spite of the apparent simplicity of the principles underlying such a system, it is nevertheless particularly difficult to achieve a robust and stable operational implementation of such a set-up with the precision required for this kind of experiment. The "simple" alignment of the components composing the system is in fact extremely restrictive, as the required range for the fringe spacing - and therefore for the beam-to-beam distance - is large. It is therefore necessary to develop a robust alignment method as well as to characterize the stability of the position of the middle fringe, which was the subject of this internship. Here is a brief chronological overview of the work achieved :

- **a first period**, from February 20 to March 24, was mainly devoted to documentation work about the experiment and the accordion lattice setup, as well as the writing of a robust and repeatable alignment procedure for this setup ; in addition, adapter plates for mounting the custom aspherical lens were designed at that time ;

- **a second period**, from March 27 to April 21, was dedicated to the installation and characterization of a prototype system for active control of the dynamics of the interference pattern using a piezoelectric transducer glued on a prototype mounting structure in aluminium and a test mirror ; this task involved realignment of the setup, as well as writing of a MATLAB program to analyse the data acquired with a beam profiler at the output of the aspherical lens ; a collaborative poster between master students of the group was also designed during this period for presentation at the Physikalisches Institut ;

- **a third period**, from April 24 to May 26, was focused on improving the data analysis program, with the implementation of more advanced functions and the robustification of the processing routine, as well as the installation of a new piezoelectric transducer, this time mounted on a proper mounting structure made of brass and with a proper specially-designed mirror ;

- **a fourth period**, from May 29 to June 14, was devoted to first recordings of the evolution of the interference pattern over short time scales (a few hundred milliseconds) and long time scale (a few hours) and to early data processing of those acquisitions.

- **finally, a fifth period**, during the whole month of July, was dedicated to the final characterization of the stability of the setup and to the writing of the report.

4.2 Alignment procedure

In order to work with an accordion lattice setup, one has to know how to align all the optical components. One of the first tasks of this internship was then to devise how to perform excellent alignment of this setup. Indeed, one wants to achieve an alignment good enough to keep the position of the interfering point after the aspherical lens constant for all the beam separations within $[5\ \text{mm}, 50\ \text{mm}]$.

To perform the alignment, two different approaches have thus been designed by Valentina Salazar Silva and myself. The first one, which is mostly the work of Valentina, consists in achieving a very precise positioning of the lens using degrees of freedom provided by a 4 or 5-axis stage placed as a support for the lens. The aim of this approach is here to reach as perfect orthogonality as possible between the beams and the entrance of the lens. Even though Valentina succeeded in getting good results with it, that method is not very robust and it is actually very long to perform (up to approximately one week in the worst case). The second method, which on the contrary seems very robust and quick to perform, consists in trying to achieve the best parallelism as possible between the two beams using a beam profiler to control the positions of the beams all the way along the propagation axis at distances as large as possible between the beam profiler and the mirrors.

Those two approaches are described here, although only very briefly regarding the first one which can be found in detail in Appendix A.

4.2.1 1st approach : orthogonality between the lens and the beams

Alignment procedure : first approach

Alignment of the bottom floor
First, one has to proceed to the alignment of the bottom floor, which mainly consists in aligning the telescopes so that the beam is as flat as possible at the output of the component and the 45° mirror mounted on linear stage.

Alignment of the back mirror
Second, one has to align the back mirror in the tower on the upper floor. To do so, one has to rotate the quarter wave plate located between this back mirror and the PBS in order to let the light come back to the lower floor and use the reflections to achieve a good alignment.

Alignment of the top mirror
Third the top mirror has to be aligned (the 45° mirror in the tower on the upper floor),

which is achieved with the help of an additional mirror placed at the exit of the PBS and set so that the reflected beams from the lower beam (so from the beam reflected by the back mirror that has just been aligned previously) overlap with the incident one. The idea is then to get overlapping between the beam coming from the top mirror and reflected by the additional mirror and its reflection.

The previous steps are quite straight-forward but it is really important to take the time to achieve them as precisely as possible.

Rough alignment of the lens
In a fourth step, the lens is mounted on top of a 4-axis stage. The main difficulty of the alignment is here as it is quite challenging to achieve an alignment of the lens that is good enough to maintain the position of the interfering point constant for all beam separations. A rough alignment is achieved first though, using a graduated piece of paper.

Rough alignment of the lens
Then, the objective is mounted and one has to make sure it is at the good position so that the light enters right at its centre.

Now, the lens can be align with more precision using the magnified image produce by the objective and observed on a piece of paper. This step takes a very long time and is quite sensitive. The alignment of the lens will be finalized using the camera though.

Fine alignment of the lens
The camera and the mirror leading to it have to be aligned then. Once this is achieved, one has to set the camera or beam profiler properly and then one can continue the alignment of the lens using the dynamics of the interference pattern while changing the beam separation after each modification of the position of the lens. As the alignment step using a piece of paper as screen, this step requires a very long time.

4.2.2 2nd approach : parallelism between the beams

Another approach to align the accordion lattice setup consists in neglecting in a first time the potential aberrations coming from the relative position of the lens with respect to the incoming beams and to consider instead the geometrical optics argument according which only matters the mutual parallelism between the two beams. Indeed, as depicted in Figure 4.1, as the two incoming beams are coming from infinity, if one is able to set the beams so that the angles α_1 and α_2 between each of them and the lens along the vertical axis are the same- let's name it α -, and so that the angles β_1 and β_2 along the horizontal axis are also the same - let's name it β -, then the position of the interfering point is only function of the latter

angles α and β. In such a configuration, a perfect orthogonality between the lens and the beams is not only no longer required but is actually not even desired anymore as one then needs the two rotational degrees of freedom around (Ox) and (Oy) to set the position of the interfering point. It is however important to note that those considerations are only valid in the small-angle approximation, so even if the lens must not be perfectly orthogonal to the beams like with the first approach, it must still be roughly orthogonal.

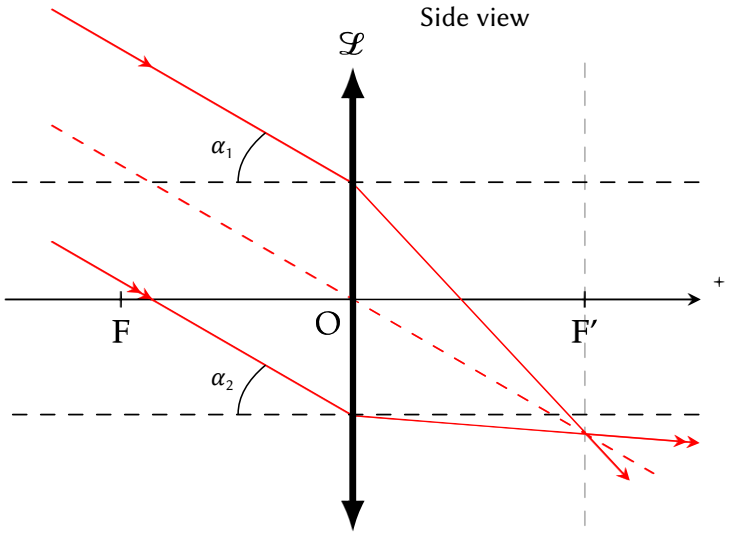

Figure 4.1: Two beams coming from infinity and meeting a focusing lens (adapted from Jimmy Roussel [51]).

In order to set as finely as possible the parallelism between the two beams, the following protocol is executed :

Alignment procedure - Second approach

Alignment of the bottom floor

First, as in the 1st approach, one has to proceed to the alignment of the bottom floor, which mainly consists in aligning the telescopes so that the beam is as flat as possible at the output of the component and the 45° mirror mounted on linear stage.

Setting of the vertical angles of the beams

In order to set the vertical angles α_1 and α_2 to the same value α, a beam profiler (Newport LBP2-HR-VIS3) is placed alternatively just after the lens (10 cm after) and as far as possible from it (3 m after) at the same height using the appropriate spacer. The vertical position of the image of each beam is then recorded at both positions and the angles made by the beams with respect to the ground slightly adjusted to correct those positions. After a few iterations of this protocol, the vertical positions of each beam is stabilized all the way after

the lens and one can conclude that the vertical angles are properly set so that each beam is parallel to the ground : the beams are thus parallel to each other and to the ground.

Setting of the horizontal angles of the beams
In order to set the horizontal angles β_1 and β_2 made by the beams with respect to the optical axis to the same value β, the beam profiler is placed after the lens so that both top and bottom beams are visible on the same image. To do so, as the imaging surface of the camera is not big enough to observe both beams entirely at the minimal beam separation, one has to set the height of the beam profiler so that half of each beams is visible as well as to set the beam separation to its minimal value in order to reach the maximum imaged proportion for each beam. A preliminary adjustment of the horizontal angles using a detector card at different locations after the lens is also required in order to see both beams on the same image with the camera. To do so, the angles are changed so that the beams get as close as possible from each other to the naked eye. Once this is done, the horizontal angles can then be set more precisely using the image from the camera.

The latter approach, undertook at the end of the internship, allows to achieve good results regarding the dynamic setting of the fringe spacing. The method used to characterise this feature consists in recording the position of the interfering point along the propagation axis (Oz) while proceeding to the compression, i.e. while scanning all the values accessible for the beam separation. In order to do so, a camera is placed on a manual translation stage along (Oz) the closest as possible to the interfering point. By fine-tuning the position of this translation stage in parallel with the observation of the interference pattern on the image from the camera, the relative position of the interference point at each stage of compression can be measured directly on the ruler of the stage.

A first characterisation undertook after setting the parallelism of the beams along a rather short distance (1 m) then gave the results showed Figure 4.2a, while a second characterisation after a better adjustment of the parallelism along the full available distance of the optical table ($\sim$ 3 m) gave better results as showed in Figure 4.2b. The error bars here are manually determined as the range of positions for which it is hard to determine with the camera if the interfering point position has been achieved or not. One should then consider this range of position as the one for which the interference pattern remains the same at the precision obtained with the camera without magnification. A more precise characterisation of that feature can be carry out using an objective to magnify the image as it is explained in the Master thesis of Valentina Salazar Silva [47].

Focusing on results from Figure 4.2b, one can see that the position of the interfering point is rather linear for beam separations between 10 mm and 50 mm (i.e. for fringe spacings between 8.0 µm and 1.6 µm) with a position difference of about 500 µm between those two beam separations. However, for beam separations smaller than 10 mm, the position of the

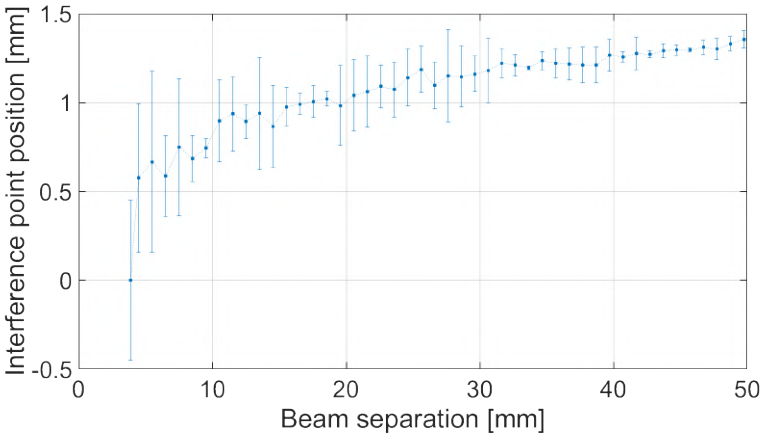

(a) After setting the parallelism along a rather short distance ($\tilde{1}$ m).

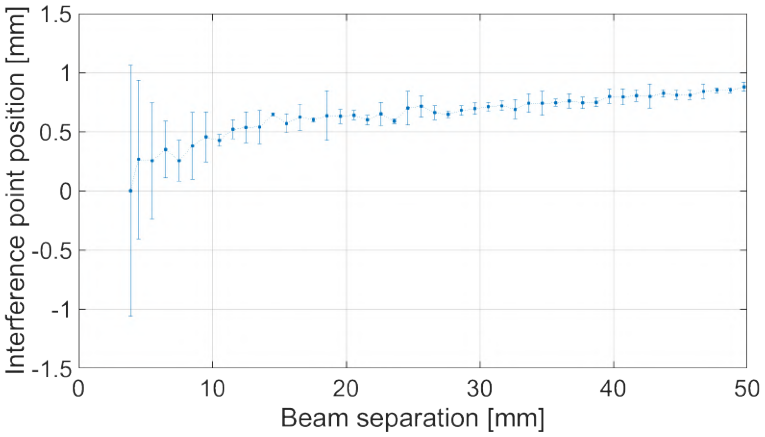

(b) After setting the parallelism along the full available distance ($\tilde{3}$ m).

Figure 4.2: Characterisations of the relative position of the interference point as a function of beam separation.

interfering point gets rather uncertain as the error bars are very wide (more than 2 µm for $D = 3.9$ mm i.e. for $d = 20.5$ µm) ; the characterisation is no longer really relevant and one needs to use the objective to get better data.

On the main experiment, as one will have to set the position of the interfering point at the exact same location as the atoms, different positioning solutions have been considered and it has not yet been decided which solution will actually be implemented. The main one, which is the one that has been implemented on the test setup and used during this internship, consists a 4(or 5)-axis stage (Newport 9071-M Four-Axis and 9081-M Five-Axis) as a support for the lens allowing translations along (Ox) and (Oy) (as well as (Oz) with the 5-axis stage) and rotations around (Ox) and (Oy). The main constraint in choosing the solution is perhaps the thickness of the stage as the height of the optical axis of the lens should exactly be 75 mmso that it is at an equal distance from the two beams. Another challenge will then consists in imaging the lattice in the science chamber as one will no longer have direct access to the interference figure. The idea is then to use another lens at the output of the science chamber

where the beams coming from the accordion escape to image this figure.

4.3 Stability tests at short and long time scales

4.3.1 How to proceed ?

To proceed to the characterisation of the stability of the interference pattern, it is necessary to develop a complete and robust data processing program to analyse the fringe movements. Two object-oriented MATLAB scripts were then developed during this internship, one containing a class *DataObj* allowing the construction and manipulation of dedicated objects for each acquisition using a set of methods specially written for this purpose, the other containing the sequence of instructions to be executed to process the data stored in these objects.

In that section, the method used to initialise all the characterisations undertaken subsequently is briefly explained. But before that, the choice of the best fringe spacing to perform the tests is discussed.

What is the best fringe spacing for performing stability tests?

As it will be explained in this section, the movement in position of the middle fringe of the interference pattern depends directly on the value of the fringe spacing. This relation can therefore be advantageously used to place the system in a configuration in which the influence of the noise on the phase is more easily quantifiable, given the larger values then taken by the noise amplitude, thereby optimising the stability tests. The theoretical calculation indicates that the most favourable situation for carrying out these tests is the configuration for which the fringe spacing is maximum.

Parameters & model :
Lets consider a series of N acquisitions taken at different times $\{t_i\}_{i\in[\![1,N]\!]}$ for the same fringe spacing d, and gathered as N realisations $\{R_i\}_{i\in[\![1,N]\!]}$.

One realisation R_i is characterized by :

- the phase difference between the two beams at time t_i :

$$\Phi_i = \varphi_{top}(t_i) - \varphi_{bottom}(t_i);$$

- the difference of this previous phase difference between realisation R_i and first realisation R_1 :

$$\Delta\Phi_i = \Phi_i - \Phi_1;$$

- the optical path length difference between the two beams at time t_i :

$$\delta_i = \mathscr{L}_{top}(t_i) - \mathscr{L}_{bottom}(t_i);$$

- the difference of this previous optical path length difference between realisation R_i and first realisation R_1 :

$$\Delta\delta_i = \delta_i - \delta_1;$$

- the position of the middle fringe at time t_i :

$$y_0(t_i);$$

- the difference of this position between realisation R_i and first realisation R_1 :

$$\Delta y_0(t_i) = y_0(t_i) - y_0(t_1).$$

With these notations, on the one hand one can write :

$$\frac{\Phi_i}{2\pi} = \frac{\delta_i}{\lambda}, \tag{4.1}$$

with λ the wavelength of the laser

So, differentiating :

$$\frac{\Delta\Phi_i}{2\pi} = \frac{\Delta\delta_i}{\lambda} \tag{4.2}$$

And on the other hand :

$$\frac{\Delta\Phi_i}{2\pi} = \frac{\Delta y_0(t_i)}{d} \tag{4.3}$$

So :

$$\frac{\Delta y_0(t_i)}{d} = \frac{\Delta\delta_i}{\lambda} \tag{4.4}$$

i.e.

$$\Delta y_0(t_i) = \frac{d\Delta\delta_i}{\lambda} \tag{4.5}$$

Therefore, as the wavelength λ is fixed and that the difference $\Delta\delta_i$ does a priori not depend on the beam separation, the variations of the position of the middle fringe only depends on the value of the fringe spacing d and one can conclude that the larger is the fringe spacing, the larger are the fluctuations of the position of the middle fringe. The best fringe spacing to proceed to stability tests is thus the maximal fringe spacing d_{max}.

Initialisation routine

Requirements

The aim of the initialisation routine is to calculate the magnification in the different acquisition planes in order to obtain the actual values of each physical quantity. This routine requires the acquisition of the following data in three different planes:

- In the **focal plane** of the lens directly: data corresponding to only one of the two beams, the other being blocked before the lens;
- In the so-called **post-objective plane**, i.e. the exit plane of a x20 objective previously placed in the focal plane of the lens in order to observe a magnified image of the interference pattern : data corresponding to an individual beam (as in the focal plane), as well as data corresponding to the interference pattern;
- In the **imaging plane**, i.e. the plane where the characterisation will be performed : data corresponding to the interference pattern only;

Each of these data sets is systematically supplemented by exactly the same number of "dark" data sets for calibration, i.e. data recorded in the same light environment as the former but with the two incident beams blocked before the lens.

Initialisation script

Once all the data have been acquired and organised as indicated in the scripts' headers, the initialisation routine can be executed. This routine consists in four main steps:

1. Processing data recorded in the focal plane :
   a) construction of an object corresponding to an individual beam in this plane ;
   b) calibration and normalisation of its intensity (Figure 4.3);
   c) vertical cross-section at the centre of the image ;
   d) Gaussian fit of this cross-section and extraction of the vertical waist in the global variable *WaistFocalPlane* (Figure 4.4);
2. Processing data recorded in the post-objective plane :
   a) construction of an object corresponding to an individual beam in this plane ;
   b) calibration and normalisation of its intensity (Figure 4.5);
   c) vertical cross-section at the centre of the image ;
   d) Gaussian fit of this cross-section and extraction of the vertical waist in the global variable *WaistPostObjectivePlane* (Figure 4.6);
   e) construction of an object corresponding to the interference figure in this plane ;
   f) calibration and normalisation of its intensity (Figure 4.7);
   g) vertical cross-section at the centre of the image ;

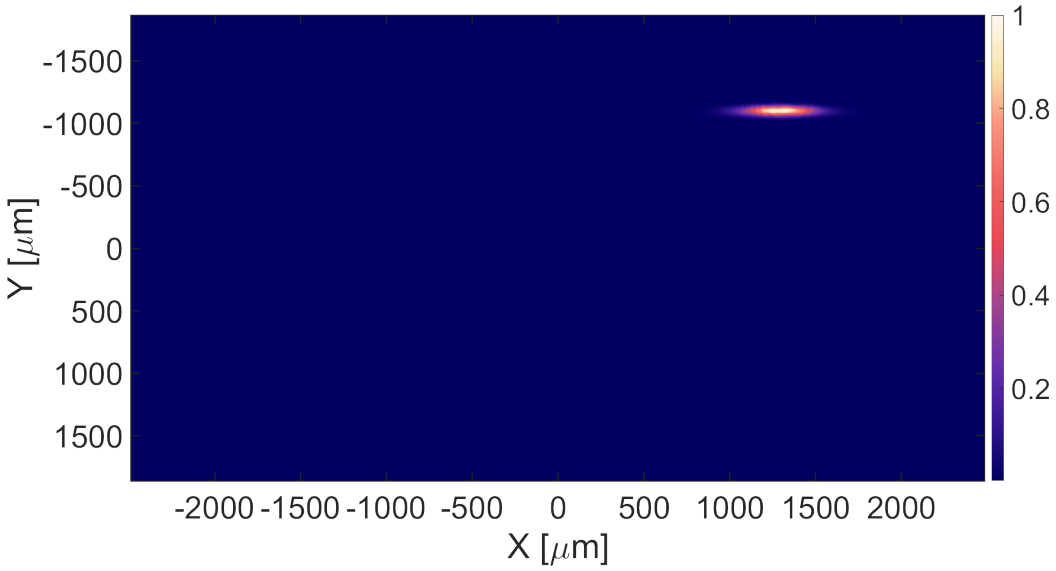

Figure 4.3: Raw data in the focal plane.

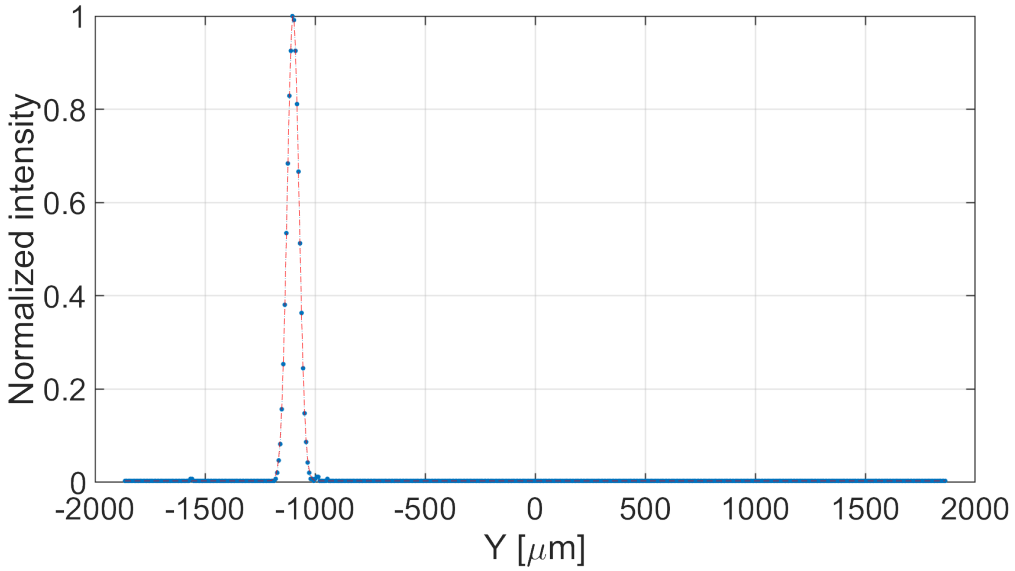

Figure 4.4: Gaussian fit of the intensity within vertical cross-section in the focal plane.

h) calculation of the Fourier transform of this vertical cross-section using FFT and extraction of the fringe spacing (spatial frequency of the cross-section) within the global variable *FringeSpacingPostObjectivePlane* ;

i) fit of this cross-section and calculation of the phase shift (Figure 4.8) ;

3. Processing data recorded in the imaging plane :

a) construction of an object corresponding to the interference figure in this plane ;

b) calibration and normalisation of its intensity (Figure 4.9);

c) vertical cross-section at the centre of the image ;

d) calculation of the Fourier transform of this vertical cross-section using FFT and

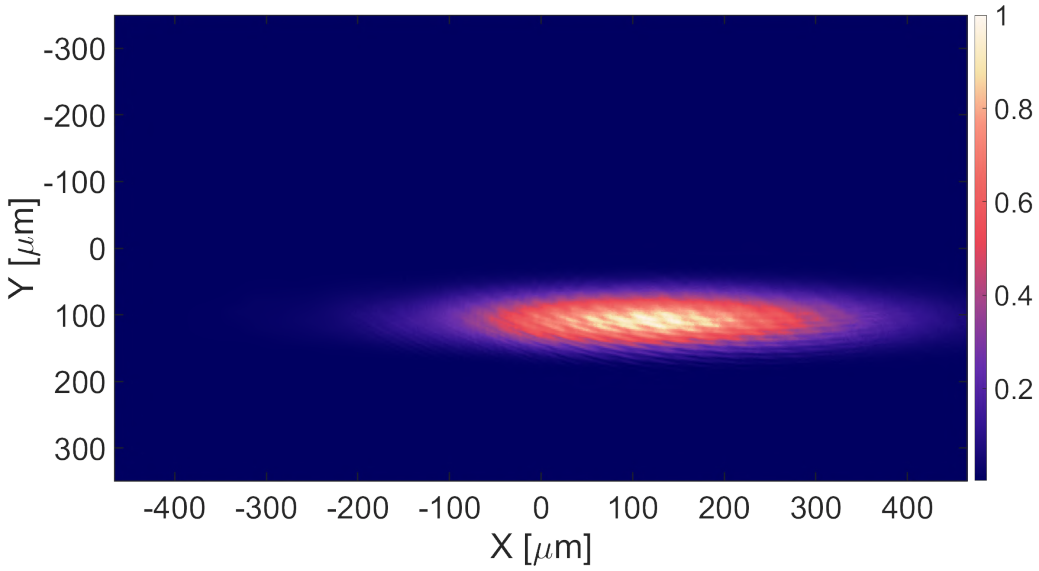

Figure 4.5: Raw data for the upper beam in the post-objective plane.

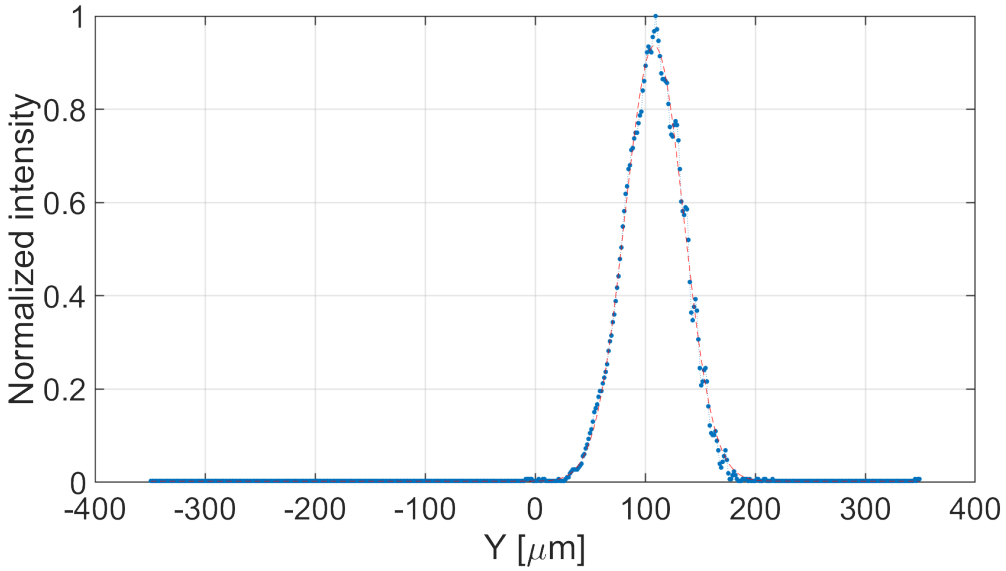

Figure 4.6: Gaussian fit of the intensity within vertical cross-section for the upper beam in the post-objective plane.

extraction of the fringe spacing (spatial frequency of the cross-section) within the global variable *FringeSpacingAcquisitionPlane* ;

e) fit of this cross-section and calculation of the phase shift (Figure 4.10).

The function used for Gaussian fits is :

$$I_g(y) = A \exp\left[-\frac{(y-\mu)^2}{2\sigma^2}\right] + D \tag{4.6}$$

And the functions used for fitting the vertical cross-section intensity are given by:

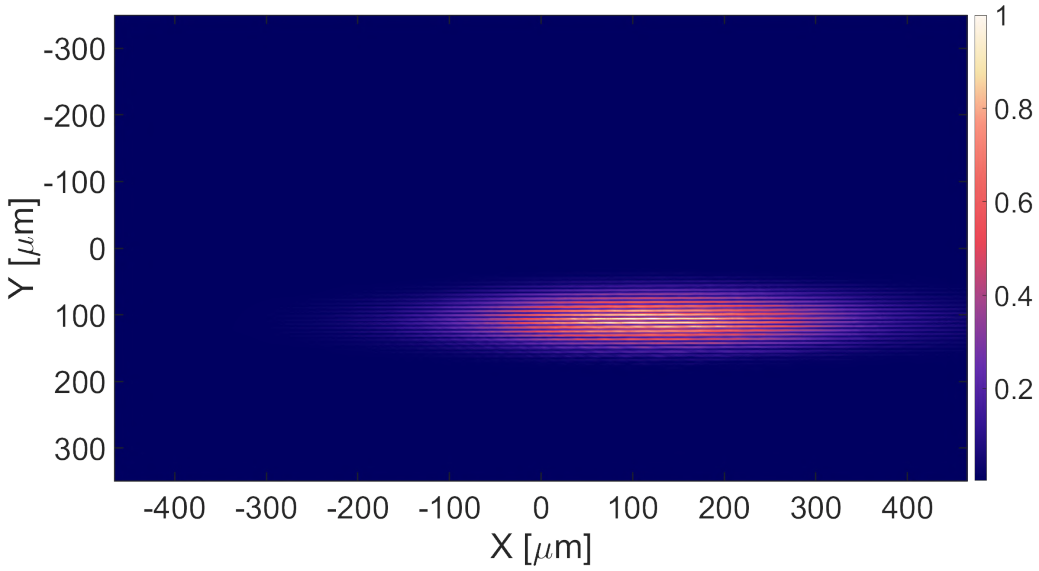

Figure 4.7: Raw data for the interference pattern in the post-objective plane.

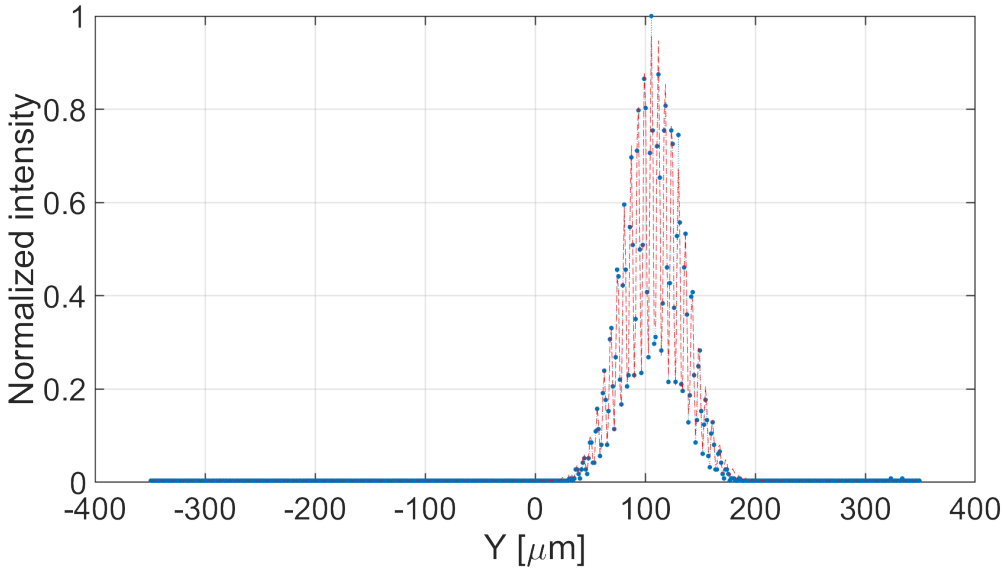

Figure 4.8: Fit of the intensity within vertical cross-section for the interference pattern in the post-objective plane.

$$\begin{cases} I(y) = A\left[1 + Ccos\left(2\pi\frac{y-y_1}{d}\right)\right]\exp\left[-2\left(\frac{y-y_0}{w_y}\right)^2\right] + B \\ I(y) = A\left[1 + Ccos\left(2\pi\frac{y}{d} + \phi\right)\right]\exp\left[-2\left(\frac{y-y_0}{w_y}\right)^2\right] + B, \quad \text{where } \phi = -2\pi\frac{y_1}{d} \end{cases} \tag{4.7}$$

These two expressions, which are strictly equivalent, are also used to extract the error in position of the principal fringe - identified by an additional method (*BatchPhaseDifference*) - as well as the error on the beam-to-beam phase shift.

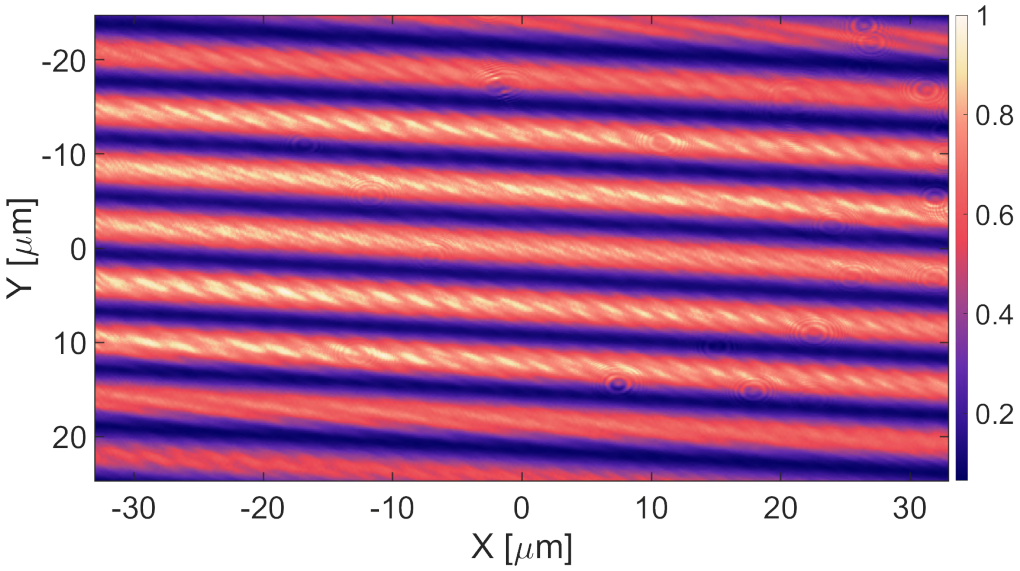

Figure 4.9: Raw data for the interference pattern in the imaging plane.

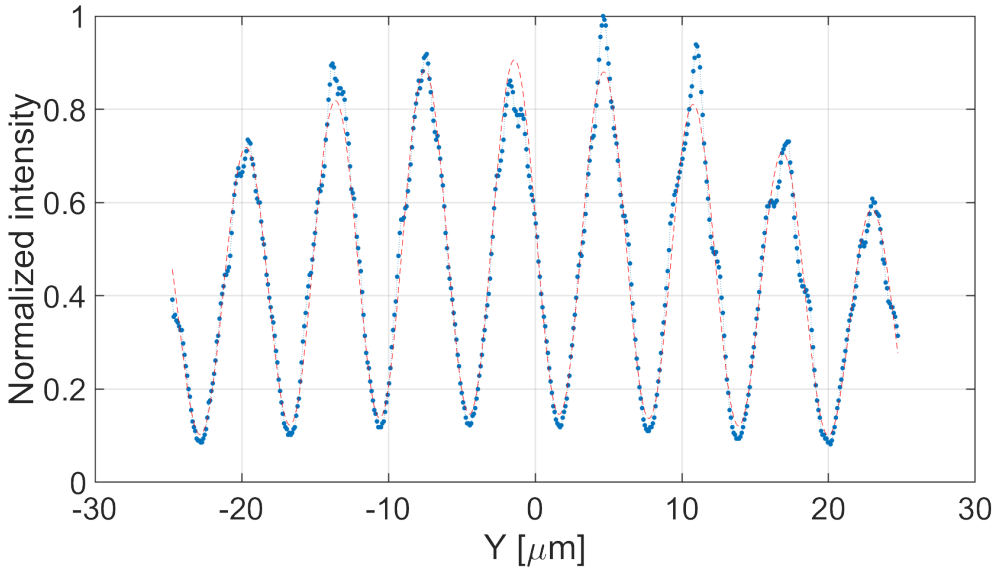

Figure 4.10: Fit of the intensity within vertical cross-section for the interference pattern in the imaging plane.

The data extracted from this initialization can then be used to calculate the magnification M in the acquisition plane for each subsequent object constructed, using the following relationship:

$$M = \frac{\text{WaistPostObjectivePlane}}{\text{WaistFocalPlane}} \times \frac{\text{FringeSpacingAcquisitionPlane}}{\text{FringeSpacingPostObjectivePlane}} \tag{4.8}$$

The initialisation routine is then complete. The characterisations can then be carried out, which is done automatically in batches by specifying the acquisition parameters at initialisation.

Characterisation routine

Extraction of the phase and calculation of the optical path length difference

The phase is extracted using three different methods: first, by fitting the theoretical expression of the interference pattern, then by fitting only the sinusoidal part of this expression, and finally by evaluating the Fourier transform of the vertical cross-section of this pattern. These different methods were developed to ensure the reliability of the results obtained, since the phase extraction algorithm initially written by considering only the complete theoretical expression was not sufficiently robust to guarantee valid results for each realisation. Although this algorithm was finally made robust by better adjustment of the starting values of the coefficients and of the research intervals of these, those methods, which still allow validation of the results, have been maintained.

Phase extraction by fitting with the complete theoretical expression

The first method consists in fitting the data with the theoretical expression of the vertical cross-section of the interference pattern :

$$I(y) = A\left[1 + C \cdot \cos\left(2\pi\frac{y}{d} + \Phi\right)\right] \cdot \exp\left[-2\left(\frac{y - y_0}{w_y}\right)^2\right] \tag{4.9}$$

Phase extraction by fitting with the sinusoidal part of the theoretical expression

The second method consists in keeping only the sinusoidal part of the expression and to fit the data with it :

$$I_{sin}(y) = \cos\left(2\pi\frac{y}{d} + \Phi\right) \tag{4.10}$$

It does not therefore provide any information other than the phase Φ and the fringe spacing d. The choice of using only this part of the expression is explained by the large number of coefficients to be determined with the complete expression, which makes the robustness of the fit more difficult.

Phase extraction by evaluation of the Fourier transform of the vertical cross-section of the interference pattern

The third and final method used to extract the phase is based on the theoretical expression of the Fourier transform of the vertical cross-section of the interference pattern.

The Fourier transform $\widetilde{I}$ of the vertical cross-section of the interference pattern writes (see Appendix B for the derivation):

$$\widetilde{I}(f) = A\sqrt{\frac{\pi}{2}} \cdot w_y \cdot \exp\left[-\frac{\pi^2 w_y^2}{2} f^2 - i2\pi y_0 f\right]\Bigg] + \frac{A \cdot C}{2} \cdot \sqrt{\frac{\pi}{2}} \cdot w_y \cdot \Bigg\{\exp\left[\frac{-\pi^2 w_y^2}{2}\left(f - \frac{1}{d}\right)^2 - i2\pi y_0\left(f - \frac{1}{d}\right) + i\Phi + \exp\left[\frac{-\pi^2 w_y^2}{2}\left(f + \frac{1}{d}\right)^2 - i2\pi y_0\left(f + \frac{1}{d}\right) - i\Phi\right]\Bigg\} \tag{4.11}$$

It can then be noticed that by evaluating this Fourier transform in $f = \frac{1}{d}$ the only remaining non-negligible term writes :

$$\widetilde{I}\left(f = \frac{1}{d}\right) \sim \frac{A \cdot C}{2} \cdot \sqrt{\frac{\pi}{2}} \cdot w_y \cdot e^{i\Phi} \tag{4.12}$$

And it is immediately clear that the phase $\widetilde{I}\left(f = \frac{1}{d}\right)$ of the Fourier transform of the vertical cross-section of the interference pattern evaluated in $f = \frac{1}{d}$ identifies with the phase Φ sought :

$$\angle\widetilde{I}\left(f = \frac{1}{d}\right) = \Phi \tag{4.13}$$

Calculation of the optical path length difference

Once the phase Φ has been extracted, it is very simple to determine the optical path length difference between the two beams using the relation $\frac{\Phi}{2\pi} = \frac{\delta}{\lambda}$, from which the following can be deduced:

$$\delta = \lambda \cdot \frac{\Phi}{2\pi} \tag{4.14}$$

Stability criteria

Criterion 1 : relation to the imaging system's depth of field

The position of the middle fringe of the accordion must vary as little as possible compared to the depth of field of the lens of the imaging system, in other words the differences Δy_0 in the position of the middle fringe must be very small compared to the depth of field ΔP of this lens. Generally speaking, the depth of field of a lens is defined as the range of distance within which an imaged object appears sufficiently sharp for the observer's criteria. It is therefore the distance $\Delta P = P_1P_2$ between the closest object P_1 to the lens that still appears sharp and the farthest object P_2 from the lens that also still appears sharp (see Figure 4.11). Considering the smallest distance Δr between two discernible points as the resolution for the lens studied here, the depth of field will thus be defined as the range of distance within which the resolution of the lens remains less than or equal to 50% of the optimum resolution (i.e. the minimum resolution $(\Delta r)_0$ obtained for an object in the focal plane).

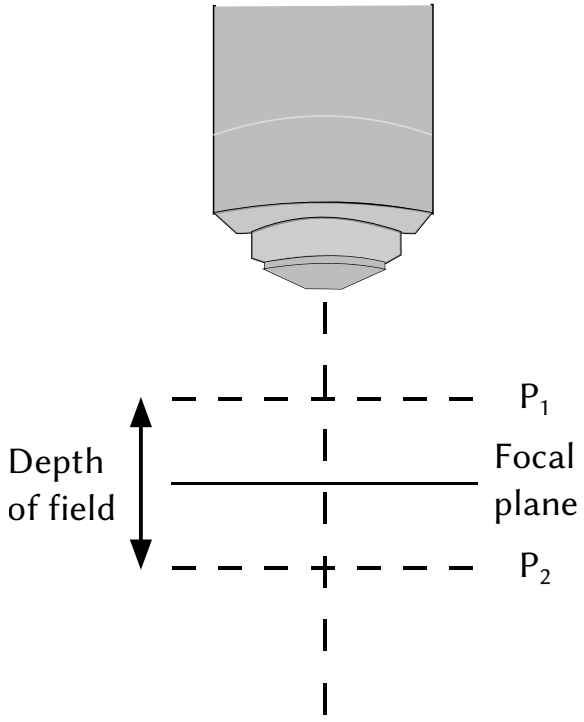

Figure 4.11: the depth of field is the distance $\Delta P = P_1P_2$ between the closest object P_1 to the lens that still appears sharp and the farthest object P_2 from the lens that also still appears sharp.

Stability criterion 1

Using these notations, a first stability criterion can be written as :

$$\Delta y_0 << \Delta P,$$

where y_0 is the position of the middle fringe of the interference pattern, Δy_0 is the variation in this position between two successive times, and ΔP is the depth of field of the imaging objective.

In terms of phases, the first stability criterion reads :

$$\varphi << \frac{\Delta P}{d},$$

with $\varphi = \frac{\Delta y_0}{d}$ the phase of the interference pattern, where d is the fringe spacing.

As the characterisation of the imaging objective has not been completed at the time this manuscript was written, the experimental value of the objective's depth of field is still unknown, but theory predicts a depth of field of the order of $(\Delta P)_{the} = 5.6$ µm according to the Master's student in charge of the project (Sarah Philips). Furthermore, as mentioned in the previous paragraph, the best configuration for performing stability tests is the configuration for which the fringe spacing is at its maximum. Although this distance was theoretically predicted to be $d_{max,the} \sim 20$ µm by Valentina Salazar Silva in her Master's thesis, the value achieved experimentally is lower, being closer to $d_{max,exp} \sim 17$ µm.

Stability criterion 1 - Numerical evaluation

With these values, the first stability criterion reads :

$$\Delta y_0 << (\Delta P)_{the} = 5.6 \text{ µm},$$

That is to say :

$$\underline{\text{Theoretical values :}} \quad \varphi << \frac{(\Delta P)_{the}}{d_{max,the}} = 0.28\text{rad} = 0.09\pi$$

$$\underline{\text{Experimental value :}} \quad \varphi << \frac{(\Delta P)_{the}}{d_{max,exp}} = 0.33\text{rad} = 0.10\pi$$

Criterion 2 : relation to the fringe spacing

It is important to avoid excessive agitation of the trapped atoms, which could lead to heating of the atoms and non-negligible loss of atoms out of the trap. One way of quantifying this is to compare the deviation in position Δy_0 of the middle fringe with the fringe spacing d.

Stability criterion 2

A second stability criterion is therefore :

$$\Delta y_0 << \frac{d}{4},$$

with again y_0 the position of the middle fringe of the interference pattern, Δy_0 the variation between two successive instants of this position, and d the fringe spacing

or, in terms of phases :

$$\varphi << \frac{1}{4},$$

with again φ the phase of the interference pattern.

Stability criterion 2 - Numerical evaluation

With the values previously established for the fringe spacing, the second stability criterion then reads :

Theoretical values : $\Delta y_0 << \frac{d_{max,the}}{4} = 5.0\ \mu m$

Experimental value : $\varphi << \Delta y_0 << \frac{d_{max,exp}}{4} = 4.2\ \mu m$

or, in terms of phases with the *experimental* value :

$$\varphi << \frac{1}{4}\text{rad} = 0.08\pi$$

4.3.2 Results of the tests and perspectives

Stability tests with a custom-shaped mounting structure for passive shifting of resonance frequencies

For preliminary testing of the piezoelectric transducer (see next section for the discussion about this feature), an aluminium mounting structure is first mounted instead of a proper brass mounting structure. This structure, described in [50], is expected to results in shifting the resonance frequencies of the mechanical system that constitutes the back mirror by adding mass to it. As the piezoelectric transducer has to remain in contact with the mirror to achieve the desired function, the aluminium structure is glued to one side of that piezo and the other side of the latter is then glued to a conventional mirror. The glue used to achieve this preliminary testing is standard one-component glue.

Once the test of the piezoelectric transducer is complete and the expected behaviour observed, a brass mounting structure is implemented. Two brass mounting structures of different masses and shapes are then available, and technical reasons it is the lightest one that is selected for implementation. The mirror used to install this mounting structure isn't a conventional mirror as before anymore. A custom-made mirror made specifically for the main experiment is instead used so that the full range of beam separations is accessible during the tests. Furthermore, in order to ensure optimum adhesion, a two-component glue is used. The mounting structure is thus carefully positioned at the centre of the mirror so that the lower beam strikes it at all the heights covered during compression. Spacers are also used at the four corners of the mirror to prevent it from slipping as the glue dries. Once the glue has dried, the system is mounted in the tower and the first measurements are made.

Stability of the interference pattern over short time scales

The first measurements consist in characterising the evolution of the beam-to-beam phase shift over time for short durations of the order of a few hundred milliseconds. The aim is thus to observe whether or not there are significant fluctuations in this phase shift - and therefore in the trap within an experimental cycle. Such fluctuations are unwanted as they may induce heating of the trapped gas.

As the maximum acquisition frequency available with the camera used is $f_{max} = 284.44\,\text{Hz}$ (i.e. a relative period $T_{min} \approx 3.5$ ms), the acquisition period is initially chosen at $T_a = 4$ ms. All the acquisition parameters are then set as follows:

- acquisition period : $T_a = 4$ ms ;
- acquisition time : $T_{tot} = 1000$ ms ;
- exposure time : $T_{exp} = 3.5$ ms ;
- gain : $G_{dB} = 7$ dB.

Data processing then gives the results Figure 4.12, showing that over a short time scale the amplitude of the fluctuations is smaller or equal to about 0.15π. Regarding stability criteria 1 and 2, the test setup is at the limit of stability with slightly higher amplitude of fluctuations that desired.

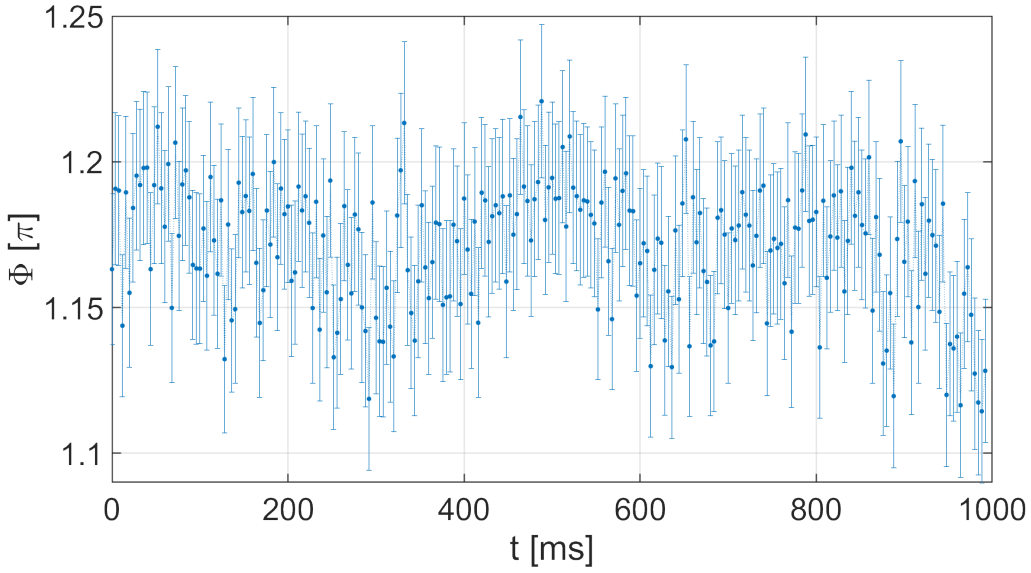

Figure 4.12: Evolution of the phase of the interference pattern over a short time scale (1000 ms).

If the amplitude of the fluctuations is resolved, it is however important to note that the frequency of these fluctuations is not. This is because this frequency is higher than the frequency of the camera.

Stability of the interference pattern over long time scales

In a second time, the evolution of the beam-to-beam phase shift over time for long durations of the order of a few hours is analysed. This is relevant to see if changes of the trap position from shot to shot will occur. The acquisition parameters used here are as follows:

- acquisition period : $T_a = 2$ min ;
- acquisition time : $T_{tot} = 2$ h ;
- exposure time : $T_{exp} = 7.8$ ms ;
- gain : $G_{dB} = 0$ dB.

The evolution of the phase of the interference pattern over a long time scale of two hours is shown in Figure 4.13.

Some strange abrupt jumps of the order of magnitude of 1π are observed, initially assumed to be due to a robustness problem in the fitting of the vertical cross-sections of the interference pattern. However, a detailed analysis of the data shows that these jumps do indeed come from the recorded data, as shown in Figure 4.14 and Figure 4.15.

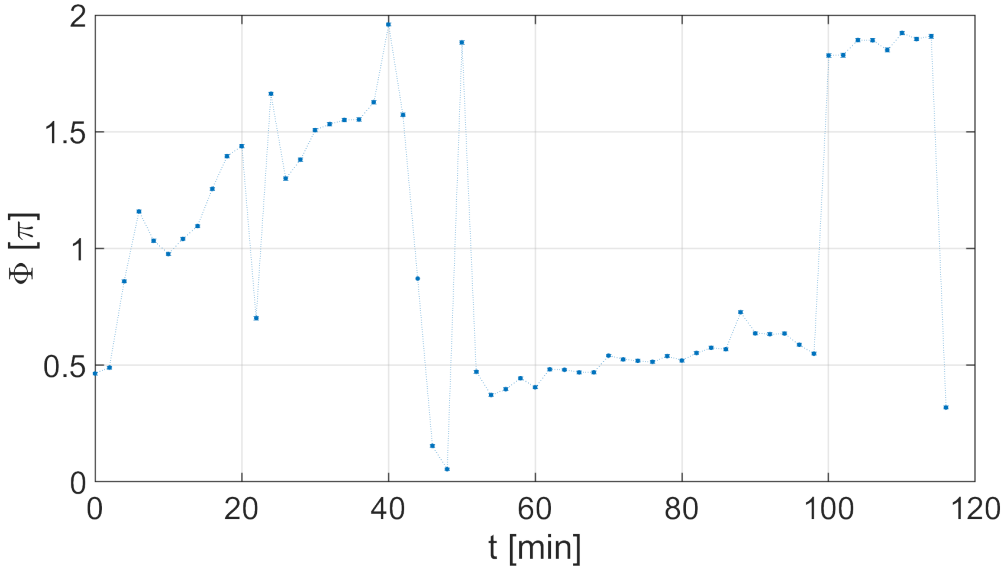

Figure 4.13: Evolution of the phase of the interference pattern over a long time scale (2 h).

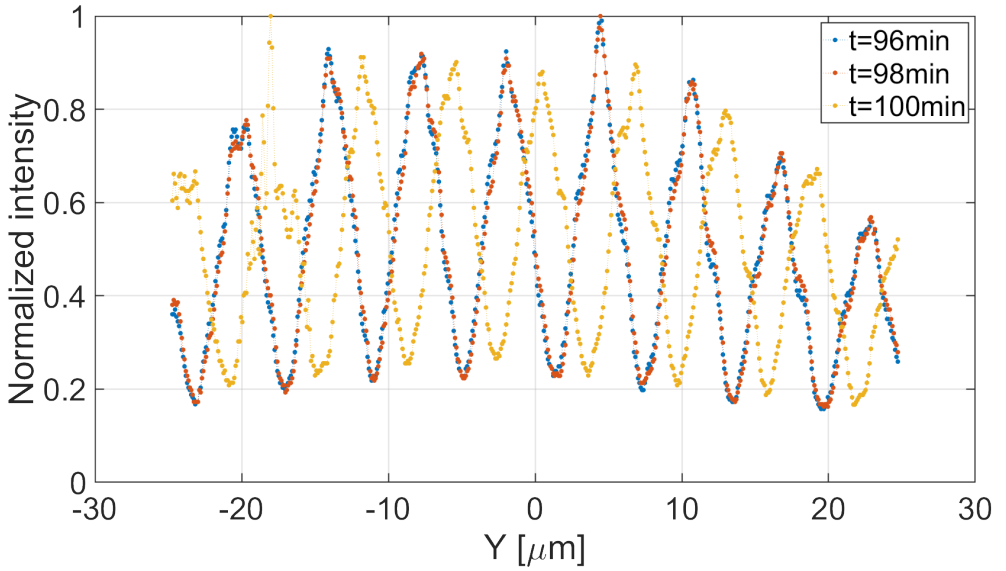

Figure 4.14: Vertical cross-section of the intensity of the interference pattern within the imaging plane at three successive moment around a jump.

In order to understand the origin of these fluctuations and to find a solution, further studies are carried out. In particular, additional acquisitions with a smaller magnification are performed to determine whether the fluctuations originate from instability of the entire interference pattern, from instability of the fringes within the pattern, or from both. The interference pattern is then recorded during six hours from 7 pm to 1 am in order to avoid vibrations coming from people working in the lab. Data processing then gives the results Figure 4.16, showing that phase jumps of the order of magnitude of about 0.3π still sometimes occur from one time to the following but not as badly as in the first test.

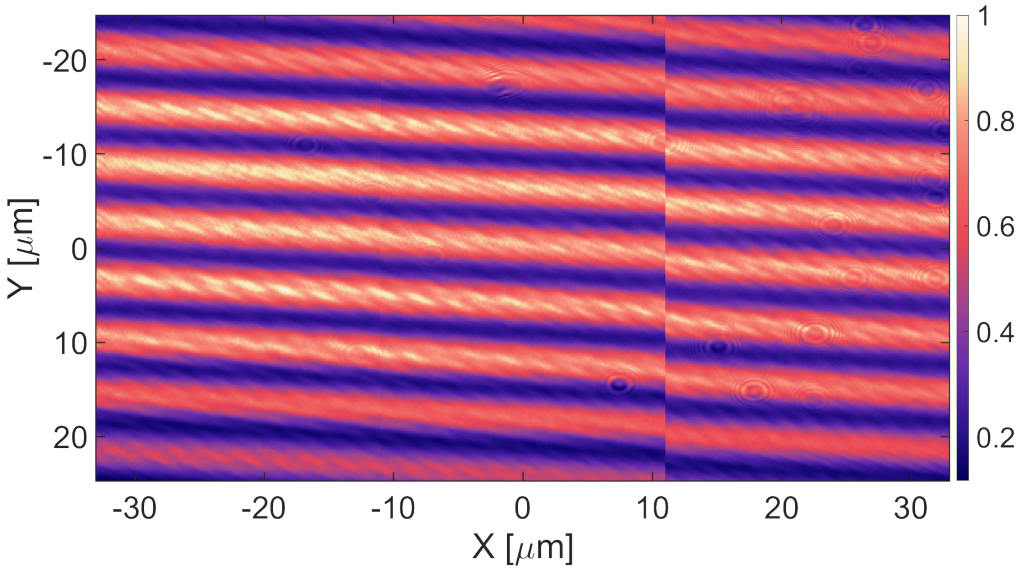

Figure 4.15: Composite image of the intensity of the interference pattern within the imaging plane at three successive moment around a jump.

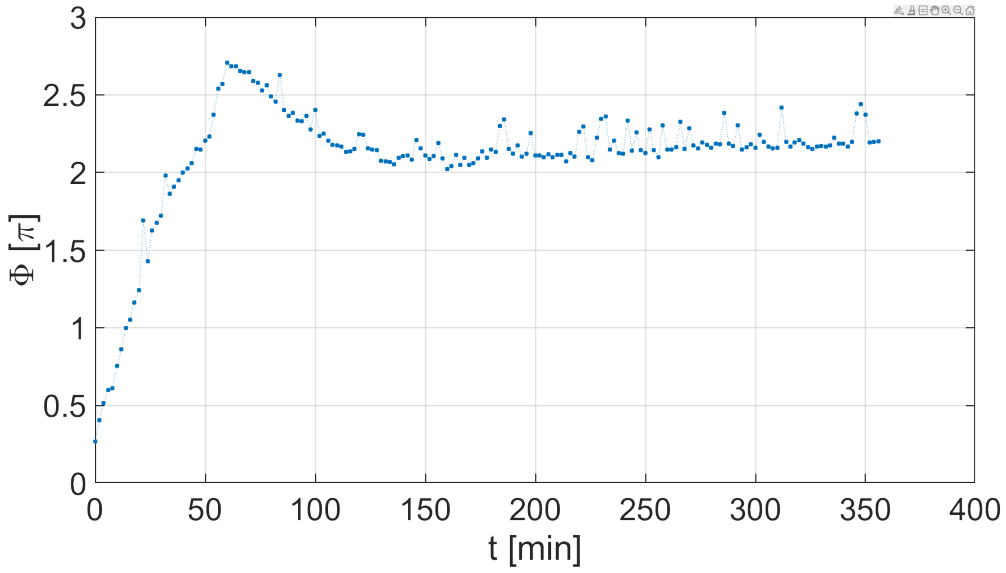

Figure 4.16: Evolution of the phase of the interference pattern over 6 h in the evening.

The amplitude of the fluctuations are although still too much regarding the criteria, so a detailed analysis is again conducted, resulting for example for the first jump at $t = 22$ min in Figure 4.17 and Figure 4.18. It is then clear that the whole figure is moving and not only the fringes within the figure. Furthermore, the analysis of the other jumps suggest the same: it is very likely that those jumps come from the displacement of the whole figure so from the stability of the mechanical structure supporting the top floor. This kind of instability is actually expected to be solved once the setup will be implemented on the main experiment so it should not be a problem.

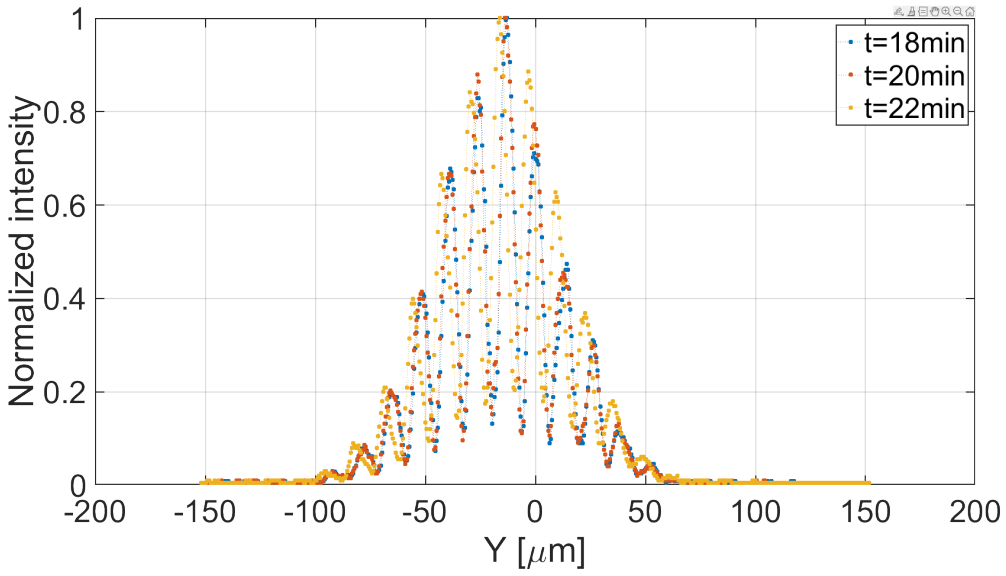

Figure 4.17: Vertical cross-section of the intensity of the interference pattern within the imaging plane around a jump at $t = 22$ min.

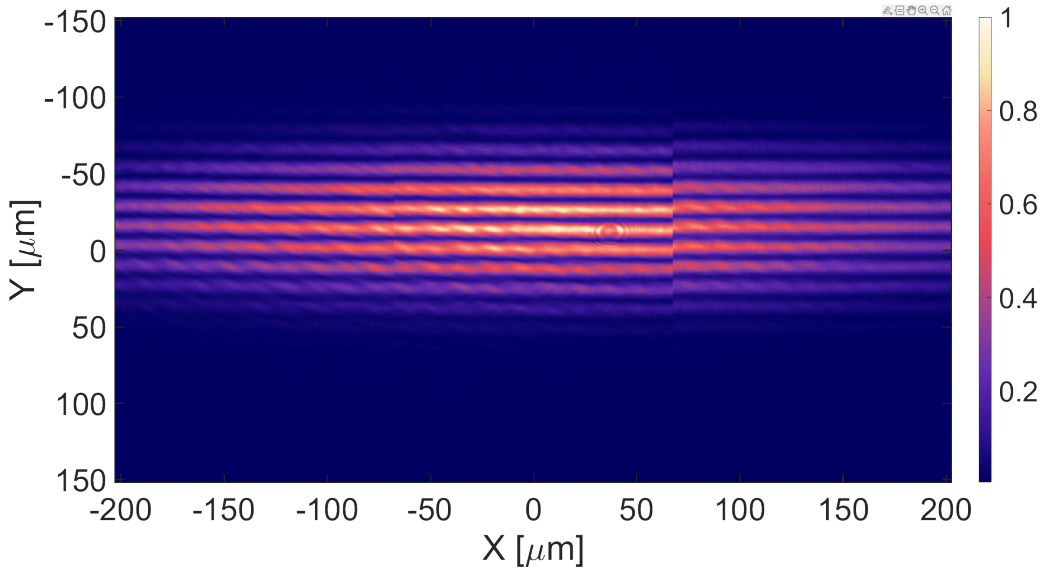

Figure 4.18: Composite image of the intensity of the interference pattern within the imaging plane around a jump at $t = 22$ min.

It is also noticeable that the phase is submitted to a long term drift of about 2π on the time scale of approximately one hour at the beginning, and then to a smaller but still important drift of about 0.7π for the rest of the recording. Because of the long time scale at which those drift are occurring and the time at which the acquisitions were done (evening), they are probably due to thermal fluctuations within the room.

Stability of the individual beams over long time scales

Thirdly, the evolution of the vertical positions of the top and bottom beams over time for long durations of the order of half a day is analysed. This is relevant to determine more convincingly whether the phase fluctuations observed previously are indeed due to instabilities of the top floor. The acquisition parameters used here are the following:

- acquisition period : $T_a = 2$ min ;
- acquisition time : $T_{tot} = 14$ h ;
- exposure time : $T_{exp} = 20$ µs ;
- gain : $G_{dB} = 0$ dB ;
- start time : 7:40 pm.

In order to observe both beams simultaneously on the camera, a Keplerian telescope with a magnification $M = 0.5$ is implemented as beam reducer. To do so, a first plano-convex lens, with focal length $f_1 = 200$ mm, is placed at the output of the PBS, and a second plano-convex lens, with focal length $f_2 = 100$ mm, is placed in the focal plane of the first one.

The evolution of the vertical positions of the center of both top and bottom beams (extracted from Gaussian fits) over fourteen hours is shown in Figure 4.19.

Fluctuations in positions between the two beams seem to be correlated, with fluctuations of amplitude of the order of 15 µm, on the one hand at very low frequencies (~ 0.1 mHz) during the first two or three hours (evening), and on the other hand at frequencies higher than the acquisition frequency ($f_a = 8$ mHz) after the third hour (night). While the low-frequency fluctuations at the beginning of the recording seem likely to be due to thermalisation of the laboratory at the end of the day when the staff leave, the origin of the higher-frequency fluctuations is not very clear.

Suspecting intuitively a linear correlation between the vertical positions of the two beams (the beams are expected to move together, constrained one with respect to the other and following the movements of the top floor), the Pearson correlation coefficient between these two quantities is calculated and the corresponding correlation diagram is plotted.

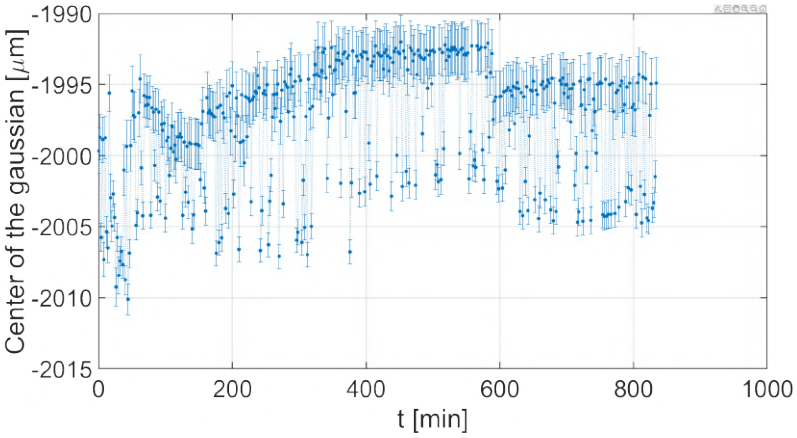

(a) Vertical position of the center of the top beam.

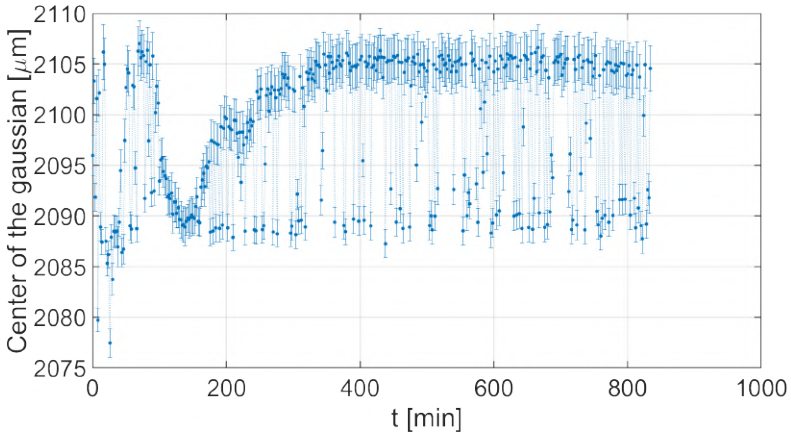

(b) Vertical position of the center of the bottom beam.

Figure 4.19: Evolution of the vertical positions of the center of both top and bottom beams over a long time scale in the evening and night (T_{tot} = 14 h ; start time : 7 : 40 pm).

Pearson correlation coefficient

The Pearson correlation coefficient indicates the presence or absence of a linear relationship between two continuous quantitative variables X and Y which respectively take their values from two finite sets $\{X_i \mid 1 \leq i \leq N\}$ and $\{Y_i \mid 1 \leq i \leq N\}$. To calculate this coefficient, it is first necessary to calculate the covariance between these two variables:

$$\mathrm{Cov}(X,Y) = \frac{1}{N-1}\sum_{i=1}^{N}\left(X_i - \bar{X}\right)\left(Y_i - \bar{Y}\right)$$

where $\bar{X}$ and $\bar{Y}$ are the expectation values of X and Y.
The linear correlation coefficient of X and Y is then equal to the covariance of X and Y divided by the product of their standard deviations σ_X and σ_Y :

$$r = \frac{\mathrm{Cov}(X,Y)}{\sigma_X \sigma_Y}$$

The correlation diagram is shown in Figure 4.20.

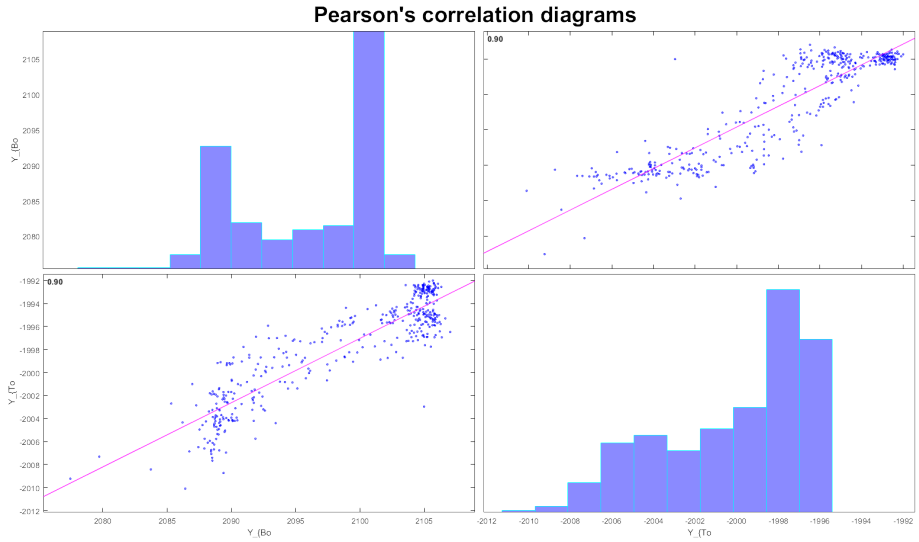

Figure 4.20: Pearson correlation diagram between the positions of the two beams.

The resulting correlation coefficient $r = 0.90$ suggests the existence of a strong and positive linear relationship between the positions of the two beams. These results therefore indicate on the one hand that the two beams move together, and on the other that the amplitude of the movements of the beams over long periods is of the order of 15 µm.

Perspectives to improve stability tests in time

As shown by the results of the tests, it is difficult to obtain precise information on the stability of the interference pattern at short times using a simple camera, particularly regarding the frequency at which phase fluctuations occur. One solution to this problem would therefore be to repeat the short-time tests not with a commercial camera but with a photo-diode in order to finally resolve this frequency.

4.4 Stability tests during compression

In order to determine the importance of orthogonality between the lens and the beams, stability tests during compression were carried out. The evolution of the phase of the interference pattern during exploration of the range of beam separations used for compression was therefore characterised - firstly without taking into account the orthogonality between the lens and the beams, and secondly trying to adjust it as accurately as possible using a 4-axis stage.

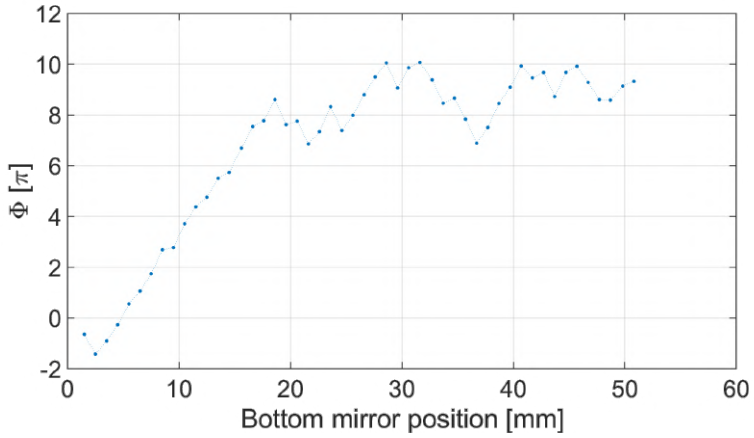

(a) Extracting the phase with the Fourier transform of the intensity.

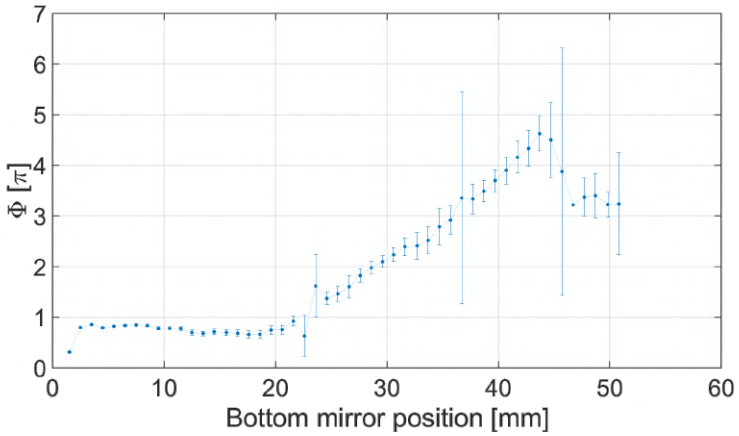

(b) Extracting the phase from the fit of the vertical cross-section.

Figure 4.21: Phase of the interference pattern as a function of beam separation during virtual compression without the 4-axis stage.

4.4.1 Stability tests without the 4-axis stage

First of all, tests were undertaken without the component that enables fine adjustment of orthogonality between the lens and the beams, i.e. the 4-axis stage. It was therefore assumed that the lens is spontaneously sufficiently orthogonal to the beams when in its custom-made mount. In other words, it was assumed that the quality of the mechanical part manufactured for the lens - as well as the quality of the surfaces of the lens itself - was good enough to achieve functional alignment without any additional degrees of freedom.

The interference pattern was therefore recorded during virtual compression within the beam separation operating range [4 mm, 50 mm]. The phase of the pattern was then extracted in the same way as for the tests of stability over time. The results are reported in Figure 4.21.

It is clear that the results are very different depending on whether they are obtained using the Fourier transform of the intensity or the fit of the intensity. This is due to the fact

that, when the phase is extracted using the fit, the fringe identified by the script as being the main one is not necessarily the same fringe from one realisation to the other. Indeed, as the magnification used to observe the fringes during the complete compression is necessarily high (of the order of x50) in order to resolve the fringes with the camera, no information on the Gaussian envelope of the interference pattern is available, and it is therefore quite difficult to determine which fringe is actually the main fringe (the script needs information on the position of the centre of the Gaussian envelope to accurately find the main fringe for all the realisations). The data presented in Figure 4.21b are therefore irrelevant.

However, looking successively at all the raw images, it seems that the position of the fringe identified as the middle one in the first realisation remains stable during compression (in other words, it seems that this fringe remains in the vicinity of its initial position for all fringe spacings). Therefore, the position of the centre of the Gaussian envelope should not vary much during compression and it can be assumed that the results obtained using the Fourier transform of the intensity are therefore relevant.

Referring to Figure 4.21a, the phase is submitted to a drift of about 10π at the beginning of compression for beam separations within [4 mm, 18 mm] (i.e. fringe spacings within [4.5 μm, 20 μm] - for more information on the relationship between beam separation and fringe spacing, see Figure 4.22), followed by fluctuations in amplitude of the order of 3π for beam separations within [18 mm, 50 mm] (i.e. fringe spacings within [1.6 μm, 4.5 μm]).

The fluctuations of the phase of the interference pattern are therefore unfortunately too high to satisfy the stability criteria established previously, as their typical amplitude is very large compared with the reference value of 0.1π.

4.4.2 Stability tests with the 4-axis stage

Tests were then carried out using a 4-axis stage to fine-tune the orthogonality between the lens and the beams. The interference pattern was again recorded during virtual compression within the beam separation operating range [4 mm, 50 mm], and the phase of the pattern was extracted as before. The results are presented in Figure 4.23.

Once again, it is clear that the results are very different depending on whether they are obtained using the Fourier transform of the intensity or the fit of the intensity - for the same reason as above: the fringe identified by the script as being the main one is not necessarily the same from one realisation to the other. The data obtained with the fit are therefore not relevant here either.

Focusing on the data obtained with the Fourier transform (Figure 4.23a), the phase appears to be submitted to a first (increasing) drift of about 7π at the beginning of compression for beam separations within approximately [4 mm, 14 mm] (i.e. fringe spacings within [6 μm, 20 μm]), followed by a second (decreasing) drift of about 12π for beam separations

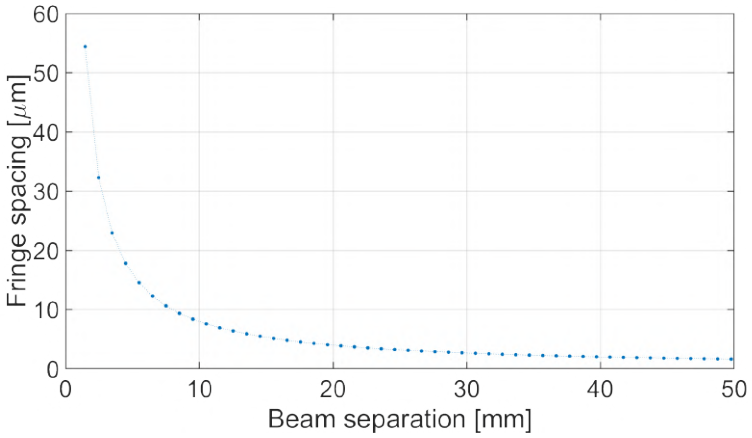

(a) Over the full operating range of the lens.

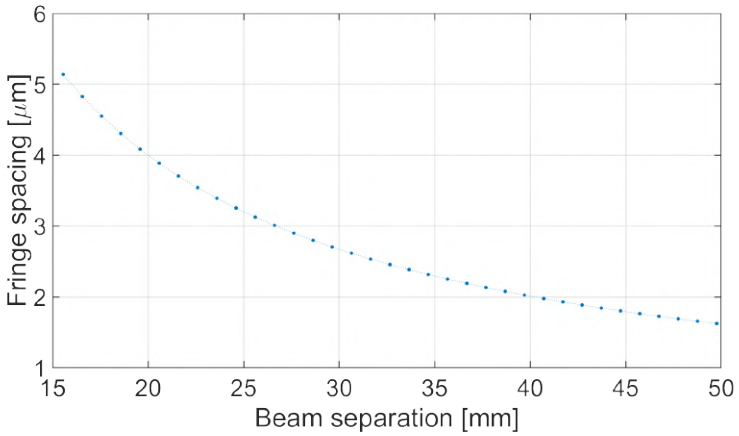

(b) For small fringe spacings.

Figure 4.22: Fringe spacing as a function of beam separation.

within [14 mm, 40 mm] (i.e. fringe spacings within [2 µm, 6 µm]). Finally, fluctuations of amplitude of the order of 1π occur for beam separations within [40 mm, 50 mm] (i.e. fringe spacings within [1.6 µm, 2 µm]).

Here too, the fluctuations of the phase of the interference pattern are too large to satisfy the stability criteria, whose reference values are of the order of 0.1π. But the most interesting information is perhaps that the alignment obtained here with the 4-axis stage is not better that the one obtained without it - although the 4-axis stage should still allow in theory better adjustment of the orthogonality between the lens and the beams, and therefore better alignment. The settings of the 4-axis stage can still be improved though.

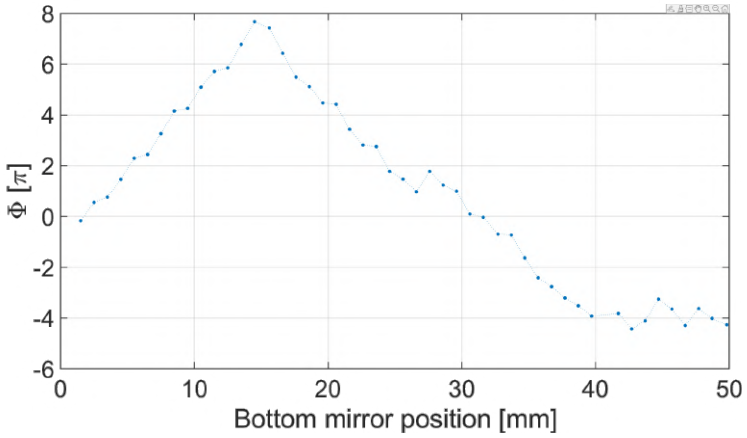

(a) Extracting the phase with the Fourier transform of the intensity.

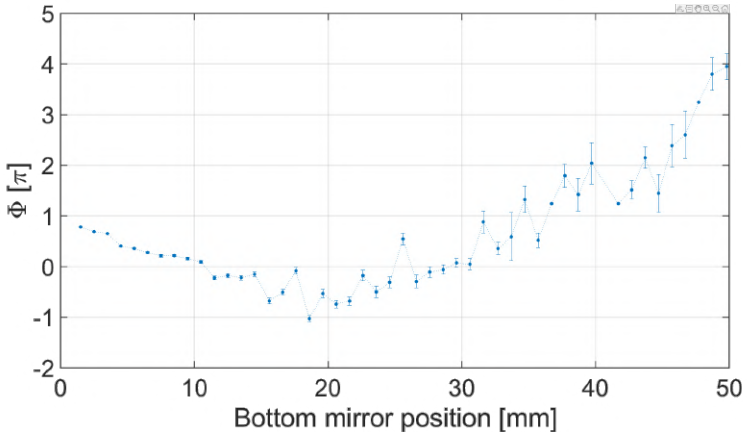

(b) Extracting the phase from the fit of the vertical cross-section.

Figure 4.23: Phase of the interference pattern as a function of beam separation during virtual compression with the 4-axis stage.

4.5 Implementation of a piezoelectric transducer

As mentioned previously, a piezoelectric transducer (Piezomechanik HPCh 150) is glued at the back of the back mirror. The idea is to use it to correct long time fluctuations of the phase of the interference figure by eventually implementing a closed-loop control system. But before to implement such a system, the transducer has to be tested.

4.5.1 Beam-to-beam phase shift as a function of the voltage

A very simple test is thus undertaken to make sure that the device works as desired, i.e. that applying a DC voltage to the input of the piezoelectric transducer indeed results in a change in the phase shift between the two beams. Different DC voltages are thus applied to the transducer, and the corresponding data are recorded using the beam profiler. The results are depicted in Figure 4.24 and Figure 4.25.

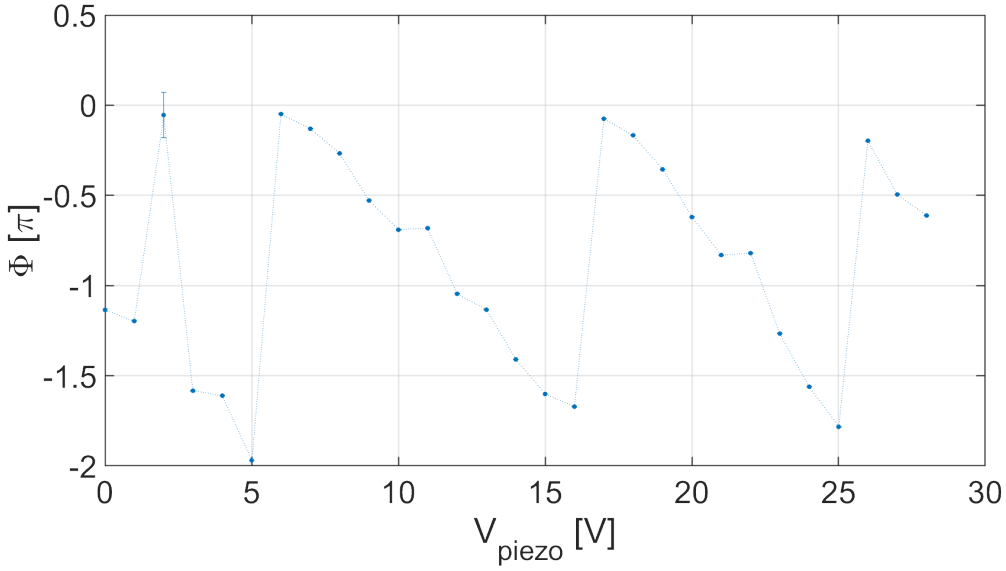

Figure 4.24: Phase of the interference pattern as a function of the applied voltage.

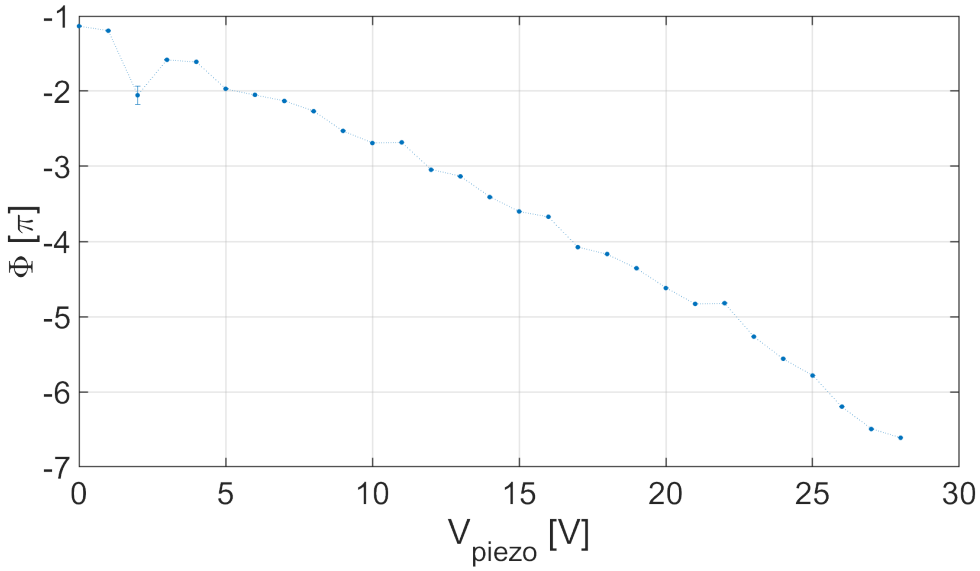

Figure 4.25: Unwrapped phase of the interference pattern as a function of the applied voltage.

This shows that the phase as a function of the applied voltage follows a piece-wise and periodic behaviour with a period of approximately $10V$ and that one can induce phase shifts of about π each time the voltage applied at the input of the piezoelectric transducer increases of approximately 5V. Giving the fact that the transducers used in the test setup allow voltages ranging from -30V to $+150V$, phase shifts between 0 and 36π can be induced.

Conclusion

This internship aimed at contributing to a dipolar quantum gases experiment conducted in the Quantum Fluids group at the Physikalisches Institut Heidelberg. It consisted in finishing to implement one of the key elements of the experiment : the accordion lattice setup. This setup, designed and built by a former Master student of the group, is intended to perform compression of three-dimensional Bose-Einstein condensates of dysprosium in order to study the physical properties of dipolar quantum systems in reduced dimensions and to investigate the physics underlying intriguing phenomena such as the Berezinsky-Kosterlitz-Thouless phase transition.

The main tasks involved the writing of an alignment procedure for the accordion lattice setup, stability tests of the position of the loading fringe over short and long time, and the implementation of a piezoelectric system to actively control the phase of the interference pattern. Indeed, instabilities in the position of the pattern may result in heating of the gas and then in atoms loss. It was therefore important to characterize the setup and to implement a system allowing real-time control of the trapping potential over time.

The stability tests showed that fluctuations of the phase of the interference pattern occurred both at short and long time scales, with some abrupt jumps measured over long time and very likely to come from the displacement of the whole figure so from the stability of the mechanical structure supporting the top floor. This kind of instability is actually expected to be solved once the setup will be implemented on the main experiment so it might not be a problem. Apart from that, phase drifts have been observed over long time, probably because of temperature fluctuations within the lab.

Bibliography

[1] M. H. Anderson et al. 'Observation of Bose-Einstein Condensation in a Dilute Atomic Vapor.' In: *Science* 269 (1995), pp. 198–201. DOI: https://doi.org/10.1126/science.269.5221.198 (cited on pages 1, 7, 12).

[2] K. B. Davis et al. 'Bose-Einstein Condensation in a Gas of Sodium Atoms'. In: *Phys. Rev. Lett.* 75 (22 Nov. 1995), pp. 3969–3973. DOI: 10.1103/PhysRevLett.75.3969 (cited on pages 1, 7, 12).

[3] Immanuel Bloch, Jean Dalibard, and Wilhelm Zwerger. 'Many-body physics with ultracold gases'. In: *Rev. Mod. Phys.* 80 (3 July 2008), pp. 885–964. DOI: 10.1103/RevModPhys.80.885 (cited on page 1).

[4] Mingwu Lu et al. 'Strongly Dipolar Bose-Einstein Condensate of Dysprosium'. In: *Phys. Rev. Lett.* 107 (19 Oct. 2011), p. 190401. DOI: 10.1103/PhysRevLett.107.190401 (cited on pages 1, 12).

[5] K. Aikawa et al. 'Bose-Einstein Condensation of Erbium'. In: *Phys. Rev. Lett.* 108 (21 May 2012), p. 210401. DOI: 10.1103/PhysRevLett.108.210401 (cited on pages 1, 12).

[6] John B. Taylor. 'Magnetic Moments of the Alkali Metal Atoms'. In: *Phys. Rev.* 28 (3 Sept. 1926), pp. 576–583. DOI: 10.1103/PhysRev.28.576 (cited on pages 1, 13).

[7] M. A. Baranov et al. 'Condensed Matter Theory of Dipolar Quantum Gases'. In: *Chemical Reviews* 112.9 (2012), pp. 5012–5061. DOI: 10.1021/cr2003568 (cited on pages 1, 15).

[8] S. Baier et al. 'Extended Bose-Hubbard models with ultracold magnetic atoms.' In: *Science* 352 (2016), pp. 201–205. DOI: https://doi.org/10.1126/science.aac9812 (cited on page 1).

[9] Fabian Böttcher et al. 'Transient Supersolid Properties in an Array of Dipolar Quantum Droplets'. In: *Phys. Rev. X* 9 (1 Mar. 2019), p. 011051. DOI: 10.1103/PhysRevX.9.011051 (cited on pages 1, 18).

[10] L. Chomaz et al. 'Long-Lived and Transient Supersolid Behaviors in Dipolar Quantum Gases'. In: *Phys. Rev. X* 9 (2 Apr. 2019), p. 021012. DOI: 10.1103/PhysRevX.9.021012 (cited on pages 1, 18).

[11] L. Tanzi et al. 'Observation of a Dipolar Quantum Gas with Metastable Supersolid Properties'. In: *Phys. Rev. Lett.* 122 (13 Apr. 2019), p. 130405. DOI: 10.1103/PhysRevLett.122.130405 (cited on pages 1, 18).

[12] URL: https://www.uni-heidelberg.de/en/university/history/heidelberg-university-nobel-laureates (cited on page 4).

[13] G. Kirchhoff. 'I. On the relation between the radiating and absorbing powers of different bodies for light and heat'. In: *The London, Edinburgh, and Dublin Philosophical Magazine and Journal of Science* 20.130 (1860), pp. 1–21. DOI: 10.1080/14786446008642901 (cited on page 4).

[14] G. Kirchhoff. *Researches on the solar spectrum and the spectra of the chemical elements [microform] / by G. Kirchhoff ; translated with the author's sanction from the Transactions of the Berlin Academy for 1861, by Henry E. Roscoe*. 1862 (cited on page 4).

[15] Isaac F. Silvera and J. T. M. Walraven. 'Stabilization of Atomic Hydrogen at Low Temperature'. In: *Phys. Rev. Lett.* 44 (3 Jan. 1980), pp. 164–168. DOI: 10.1103/PhysRevLett.44.164 (cited on pages 7, 10).

[16] Steven Chu et al. 'Three-dimensional viscous confinement and cooling of atoms by resonance radiation pressure'. In: *Phys. Rev. Lett.* 55 (1 July 1985), pp. 48–51. DOI: 10.1103/PhysRevLett.55.48 (cited on pages 7, 11).

[17] Eric A. Cornell, Jason R. Ensher, and Carl E. Wieman. *Experiments in Dilute Atomic Bose-Einstein Condensation*. 1999 (cited on page 7).

[18] Claude Cohen-Tannoudji, Jean Dalibard, and Franck Laloë. 'Chapitre 3. La condensation de Bose-Einstein dans les gaz'. FR. In: *Einstein aujourd'hui*. Savoirs Actuels. Les Ulis: EDP Sciences, 2005, pp. 89–127 (cited on page 7).

[19] Nick P. Proukakis, David W. Snoke, and Peter B. Littlewood, eds. *Universal Themes of Bose-Einstein Condensation*. Cambridge University Press, Jan. 2017 (cited on page 7).

[20] H. Kamerlingh Onnes. 'The liquefaction of helium.' In: *Proceedings* 11 (1909), pp. 168–185 (cited on page 7).

[21] Dirk van Delft and Peter Kes. 'The discovery of superconductivity'. In: *Physics Today* 63.9 (Sept. 2010), pp. 38–43. DOI: 10.1063/1.3490499 (cited on page 7).

[22] P. Kapitza. 'Viscosity of Liquid Helium below the λ-Point'. In: *Nature* 141.3558 (Jan. 1938), pp. 74–74. DOI: 10.1038/141074a0 (cited on page 8).

[23] J. F. Allen and A. D. Misener. 'Flow Phenomena in Liquid Helium II'. In: *Nature* 142.3597 (Oct. 1938), pp. 643–644. DOI: 10.1038/142643a0 (cited on page 8).

[24] Bose. 'Plancks Gesetz und Lichtquantenhypothese'. In: *Zeitschrift für Physik* 26.1 (Dec. 1924), pp. 178–181. DOI: 10.1007/bf01327326 (cited on page 8).

[25] A Einstein. 'Quantentheorie des einatomigen idealen Gases, Sitzungsberichte/Physikalische Klasse'. In: *Preussische Akademie der Wissenschaften* 22 (1924) (cited on page 8).

[26] A Einstein. 'Quantentheorie des einatomigen idealen Gases. II, Sitzungsberichte/-Physikalische Klasse'. In: *Preussische Akademie der Wissenschaften* 1 (1925) (cited on page 8).

[27] Abraham Pais. *Albert Einstein: La vie et l'oeuvre "Subtil est le Seigneur"*. fr. 2005 (cited on page 9).

[28] Willian C. Stwalley and L. H. Nosanow. 'Possible "New" Quantum Systems'. In: *Phys. Rev. Lett.* 36 (15 Apr. 1976), pp. 910–913. DOI: 10.1103/PhysRevLett.36.910 (cited on page 9).

[29] Charles E. Hecht. 'The possible superfluid behaviour of hydrogen atom gases and liquids'. In: *Physica* 25.7-12 (Jan. 1959), pp. 1159–1161. DOI: 10.1016/0031-8914(59)90035-7 (cited on page 9).

[30] T.W. Hänsch and A.L. Schawlow. 'Cooling of gases by laser radiation'. In: *Optics Communications* 13.1 (1975), pp. 68–69. DOI: https://doi.org/10.1016/0030-4018(75)90159-5 (cited on page 10).

[31] D. J. Wineland and H. Dehmelt. 'Proposed 1014 $\nu < \nu$ laser fluorescence spectroscopy on TI+ mono-ion oscillator III'. In: *Bulletin of the Americal Physical Society* 20 (1975) (cited on page 10).

[32] Jimmy Roussel. *Introduction au laser*. Apr. 2014 (cited on pages 10, 11).

[33] T Lahaye et al. 'The physics of dipolar bosonic quantum gases'. In: *Reports on Progress in Physics* 72.12 (2009), p. 126401. DOI: 10.1088/0034-4885/72/12/126401 (cited on pages 12, 16).

[34] Jean Dalibard. *Les interactions entre atomes dans les gaz quantiques: De l'universalité de van der Waals aux résonances de Fano–Feshbach*. 2021 (cited on pages 13–15).

[35] Thorsten Köhler, Krzysztof Gó ral, and Paul S. Julienne. 'Production of cold molecules via magnetically tunable Feshbach resonances'. In: *Reviews of Modern Physics* 78.4 (2006), pp. 1311–1361. DOI: 10.1103/revmodphys.78.1311 (cited on page 15).

[36] Cheng Chin et al. 'Feshbach resonances in ultracold gases'. In: *Reviews of Modern Physics* 82.2 (2010), pp. 1225–1286. DOI: 10.1103/revmodphys.82.1225 (cited on page 15).

[37] Holger Knieling et al. 'Growth of surface undulations at the Rosensweig instability'. In: *Phys. Rev. E* 76 (6 Dec. 2007), p. 066301. DOI: 10.1103/PhysRevE.76.066301 (cited on page 16).

[38] G. V. Chester. 'Speculations on Bose-Einstein Condensation and Quantum Crystals'. In: *Phys. Rev. A* 2 (1 July 1970), pp. 256–258. DOI: 10.1103/PhysRevA.2.256 (cited on page 17).

[39] Fabian Böttcher. *Supersolid arrays of dipolar quantum droplets*. en. 2020 (cited on page 17).

[40] Eugene P. Gross. 'Unified Theory of Interacting Bosons'. In: *Phys. Rev.* 106 (1 Apr. 1957), pp. 161–162. DOI: 10.1103/PhysRev.106.161 (cited on page 18).

[41] Giovanni Modugno. 'Fundamental properties of supersolids in a dipolar quantum gas'. In: ECTstar, June 2022 (cited on page 18).

[42] Henrik Jeldtoft Jensen. *The Kosterlitz-Thouless Transition*. URL: https://www.mit.edu/~levitov/8.334/notes/XYnotes1.pdf (cited on page 18).

[43] W. Ketterle, D. S. Durfee, and D. M. Stamper-Kurn. *Making, probing and understanding Bose-Einstein condensates*. 1999 (cited on page 19).

[44] Shuwei Jin et al. *A 2D MOT of dysprosium atoms as a compact source for efficient loading of a narrow-line 3D MOT*. 2023 (cited on page 19).

[45] Rudolf Grimm, Matthias Weidemüller, and Yurii B. Ovchinnikov. *Optical dipole traps for neutral atoms*. 1999 (cited on page 20).

[46] J. Dalibard Z. Hadzibabic. 'Two-dimensional Bose fluids: An atomic physics perspective'. In: *La Rivista del Nuovo Cimento* 34 (6 2011). DOI: 10.1393/ncr/i2011-10066-3 (cited on page 20).

[47] Valentina Salazar Silva. 'The Accordion Lattice: Towards Trapping of Dysprosium Ultracold Gases in Two Dimensions.' In: *Master's Thesis* (2023). University of Heidelberg, Germany (cited on pages 20, 22, 24, 29).

[48] T. C. Li et al. 'Real-time control of the periodicity of a standing wave: an optical accordion'. In: *Opt. Express* 16.8 (Apr. 2008), pp. 5465–5470. DOI: 10.1364/OE.16.005465 (cited on page 20).

[49] J. L. Ville et al. 'Loading and compression of a single two-dimensional Bose gas in an optical accordion'. In: *Phys. Rev. A* 95 (1 Jan. 2017), p. 013632. DOI: 10.1103/PhysRevA.95.013632 (cited on page 20).

[50] E. Magnan et al. 'A low-steering piezo-driven mirror'. In: *Review of Scientific Instruments* 89.7 (July 2018). 073110. DOI: 10.1063/1.5035326 (cited on pages 24, 43).

[51] Jimmy Roussel. *Cours d'optique géométrique*. 2021 (cited on page 28).

[52] Lauriane Chomaz et al. 'Dipolar physics: a review of experiments with magnetic quantum gases'. In: *Reports on Progress in Physics* 86.2 (2022), p. 026401. DOI: 10.1088/1361-6633/aca814.

[53] Louis Lafforgue. 'Study of a dipolar gas confined in a one-dimensional lattice and construction of a new imaging setup for the ERBIUM experiment'. In: *Master's Thesis* (July 2022).

[54] Nicolò Antolini. 'Towards Strongly Dipolar Superfluids in Two Dimensions'. In: *Master's Thesis* (2021). University of Florence, Italy.

[55] Travis C. Briles et al. 'Simple piezoelectric-actuated mirror with 180 kHz servo bandwidth'. In: *Opt. Express* 18.10 (May 2010), pp. 9739–9746. DOI: 10.1364/OE.18.009739.

[56] H. D. Zeh. 'On the interpretation of measurement in quantum theory'. In: *Foundations of Physics* 1.1 (1970), pp. 69–76. DOI: 10.1007/bf00708656.

Appendix A : Alignment procedure

Initial advices :

To align the setup, a vertical graduated rule with horizontal cuts on the borders was initially used. Therefore, when aligning beams, one can be tempted to trust the symmetry offered by this graduated rule, but this is not good! Indeed, as it was handmade for guiding purpose and not for precise alignment, it is not sufficiently accurate to achieve properly the alignment. One should thus remember to better trust the (mis)alignment indications that can be read all along the optical path at each points where both the incident and reflected beams are visible (the so-called "alignment check points") and check if those overlap correctly.

Remember :

Better trust the alignment check points rather than the beams' symmetry on the graduated rule!

1 Alignment of the bottom floor

1. Remove the bottom translation stage block as a whole ;
2. Align the bottom floor's mirrors so that the beam's height is the same all along the path ;
3. Set the telescopes so that the output beam at the very end is the flattest and the most parallel to the ground as possible (check it as far as possible from the output) ;
4. Then, on the top floor, block the top and back mirrors and put the bottom translation stage block back to its place ;
5. Align this block roughly so that the beam goes up to the top floor passing through the middle line of the PBS ;
6. Proceed to the fine alignment of the bottom mirror so that the incident beam and the reflected beams overlap ;
7. Then do not touch the bottom mirror anymore !

2 Alignment of the back mirror

Last check point :
Bottom stage mirror aligned ; both top and back mirrors are masked.

1. Unblock the back mirror and align it with respect to the bottom mirror so that the incident and reflected beams overlap ;

   > **Attention** : To do so, one has to remove the wave plate between the PBS and the back mirror - otherwise, due to polarization filtering, the beam of interest can't go back down to the bottom floor !
   >
   > Note : In the piezo configuration, it is difficult if not impossible to remove the wave plate so, instead, loose the screws fixing the wave plate and rotate it so that the intensity of the beam going out along the propagation axis is as low intensity as possible - and so that the beam going back down is as high intensity as possible.

2. Then check the vertical height of the lower beam (i.e. the beam coming from the back mirror) after the PBS at several positions, and slightly adjust the back mirror if the vertical height of the beam is not constant (and then check again the alignment of the back mirror with respect to the bottom mirror) ;

3 Alignment of the top mirror

Last check point :
Back mirror aligned ; top mirror is masked. For more explanations about how to achieve the previous steps, refer also to Valentina Salazar Silva's Master thesis.

1. Clear the way after the output of the PBS ;
2. Put the 2-inch mirror as far as possible from the output of the PBS and face to it ;
3. Using the screws of the 2-inch mirror, align the mirror so that the retro reflected beam coming from the bottom beam overlap properly with the incident bottom beam using the graduated rule at several positions all along the propagation axis so that the incident bottom beam passes through the corner of a cut part of the rule (this way, one can observe both the incident and reflected beams directly on the rule looking at each side of it - the incident one being observable on the input side of the rule and the retro reflected one on the output side) ;

4. Once this is fine, unmask the top mirror and align it : one can then make the top beam parallel to the bottom beam, putting the graduated rule as far as possible from the output of the 2-inch mirror (so basically in front of the PBS) at (again) a position allowing the passage of the incident beam at the corner of a cut part of the rule. To do so (i.e. to achieve 'symmetry between'/'vertical alignment of' the top and bottom beams), one has to use the back screw of the top mirror (which is the one that control the vertical position of the top beam).

   Notes :

   - When aligning the top mirror, one can still very slightly change the orientation of the back mirror if one notices that the beam is not very parallel to the ground (when looking at several different positions from the back mirror all long the axis up to optical infinity).
   - The parallelism between the beams can also be improved by slightly adjusting, if necessary, the angle of the telescope lenses.

4 Rough alignment of the lens

Last check point :
Beams are shaped at the output of the PBS (just before the lens).

Two methods are described in Valentina Salazar Silva's Master thesis ; both are useful to achieve a good alignment.

4.1 Method 1 : flipping the lens

Valentina found that this method is less accurate that the 2nd one ; nevertheless, it still gives a good basis for the achievement of an accurate alignment afterwards with the 2nd method, so it is useful to do it.

1. Flip the whole stage of the lens around so that the flat face of the lens is at the output of the PBS ;
2. Then try to achieve the alignment of the flat face of the lens using the retro reflections of the output beams from the PBS on this face (there are four of them). As the lens will have to be flipped back to its initial position, one can only adjust its vertical position ; to do so, use the bottom screws of the translation stage ;

a) Achieve overlapping of the centre reflections and symmetry of the outer reflections between the retro reflected beams coming from the aspherical face of the lens (which are the two outer beams, i.e. the top one and the bottom one) ;

b) Then adjust the position of the retro reflected beams coming from the flat face of the lens (which are the two inner beams) so that they end up being symmetric ;

c) Repeat the last two steps until symmetry is achieved and all beams are vertically aligned ;

3. Then flip the lens back to the correct position ;

   If the inner beams are not properly horizontally aligned with respect to each other, it might come from the alignment of the top mirror ; one can thus slightly change the settings of this mirror using the front screw ;

4. Improve the vertical alignment using the retro reflections on both the flat face (which is now after the aspherical part) and the aspherical face ;

   > Note : now there are four reflected beams, a group of two at the edges of the figures coming from retro reflections on the aspherical face of the lens, and another group of two at the centre of the figure coming from retro reflections on the flat face of the lens.

   a) Use first the graduated rule to set the screws of the lens's stage so that the two incoming beams (which are visible by looking at the input of the graduated rule) and the two retro reflected beams from the flat face of the lens (which are visible by looking at the output of the graduated rule through the horizontal cuts on its border) overlap roughly (without touching any other screws that those of the translation stage) ;

   b) Check the symmetry of the beams coming out of the lens by looking at the vertical position of the focal point ;

   c) Iterate those steps using alternately the top left screw and the top right screw again and again until the vertical alignment is achieved.

5. One can then proceed to the horizontal alignment, putting the graduated rule between the PBS and the lens so that the retro reflected beams and the incident beams are at the vertical edge of the rule. To do so, align the retro reflected beams (visible on the output face of the rule) with the incident beams (visible on the input face of the rule) using the top screws of the lens's stage.

4.2 Method 2 : without flipping the lens

It seems that this method is more accurate regarding the shift of the focal point when exploring the range of positions of the bottom translation stage, but it might be necessary to perform a first raw alignment of the lens using method 1 to be able to perform method 2.

1. Clear the way out after the PBS ;
2. Put a mirror (2-inch mirror for example) on the linear stage ;
3. Alignment of the mirror mounted on the linear stage with respect to the bottom beam (the mirror mounted on the linear stage will be referred to as 'end mirror') :
    a) Block the top beam by masking the top mirror ;
    b) Using the end mirror's screws, align the end mirror with respect to the bottom beam, so make the retro reflected beam coming from the end mirror and the incident beam coming from the back mirror overlap at each available alignment check points.
4. Alignment of the top beam with respect to the end mirror :
    a) Unmask the top mirror and then mask the back mirror ;
    b) Align the top beam using the top mirror's screws by making the retro reflection coming from the end mirror overlap with the incident beam from the top mirror at each available alignment check points.
5. Then put the lens back ;
6. Put the graduated rule just after the PBS and set the screws of the lens's stage roughly so that the retro reflected beams coming from the end mirror are vertically and horizontally symmetric ;
7. Then put the graduated rule after the lens and look for the position of the linear stage corresponding to the focal point, so that the end mirror ends up at the focal point :
    a) Put the rule after the lens at a position such that the incident beams coming from the lens pass through edges of the little cuts in the rule and thus meet afterwards the end mirror in partial transmission (so that both the incident beams on the input of the rule and the retro reflected beams on the output of the rule are visible) ;

Notes :

- Incident beams must meet edges of the little cuts of the rule, not the centre of the cuts, otherwise transmission is total and the incident beams are no longer visible on the rule.
- If there are no positions allowing this configuration, change the beam separation by translating the bottom translation stage.

b) Then play with the translation screw of the linear stage to find the position of the end mirror corresponding to the focal point of the lens, i.e. the position for which the incident beams and the retro reflected beams overlap on both sides of the rule.

Tip to place the rule :

- Place the rule after the last position for which the incident beams are transmitted.
- Then, carefully, move the rule back very slightly until one can observe intense retro reflected beams at the output of the rule.
- Then move the linear stage so that the incident and retro reflected beams overlap.

8. Then put the rule just after the PBS and block the back mirror so that all the visible beams come from the beam that is reflected by the top mirror(except the incident one, that comes from the bottom stage) ;
9. Then move the screws of the lens's stage so that the retro reflected beams and the incident beams overlap properly at each available alignment check points ;
10. Put the rule after the PBS so that the top beam passes completely through the centre of a cut of the rule ;

Note : If there are no such positions, change the beam separation by translating the bottom translation stage.

11. Then follow the path of this beam to identify the corresponding beam on the output of the rule ;
12. Knowing which beam is the incident one and which beam is the retro reflected one, use the screws of the lens's stage to make those beams overlap at each available alignment check points before the PBS.

Notes :

- The alignment check points can only be used before the aspherical part of the lens. After this part, the graduated rule must be used instead, keeping in mind that the positions of the beams on it are not absolute but relative. Therefore, symmetry must be achieved between the appropriate beams, rather than overlap of the beams as sought at alignment check points.
- It can be difficult to identify the retro reflected beam of interest at alignment check points here, so one should follow this rule : the less reflection, the better anyway!
- When it is not clear how to improve the settings, have a look at the beams on the PBS and make the reflected and incident beams overlap on the cube directly.
- For the horizontal alignment (at the end of the process), when looking at the input of the rule placed before the end mirror, one can particularly rely on the horizontal alignment of the outer beams, which are those which have the longest optical path so that give the best indications for misalignment.
- When looking at the output of the rule placed between the PBS and the lens, one can follow the following relation :

  a) Inner retro-reflected beams symmetry (both vertically and horizontally) tells you about the tilt of the lens, as those beams come from the reflection of the incident beams on the flat face of the lens (back face then) ;

  b) Outer retro-reflected beams symmetry tells you about the centring of the lens with respect to the incident beams, as those beams come from the reflection of the incident beams on the aspherical face of the lens (front face then).

5 Alignment of the objective

Last check point :
Lens roughly aligned.

1. First, one has to find out what is the exact height of the proper-optical-axis (i.e. the axis for which incoming beams at the input of the lens are equidistant). The position of the entrance point of the objective needs to be very precisely set on this axis, so that it can be used afterwards to finely align the lens. A misalignment of the lens would indeed bend the optical axis at the output of the lens, which would then be noticeable by simply looking at the height at which the two outcoming beams of the lens meet (this meeting point must therefore be exactly at the centre of the entrance point of the objective).

> Note : check the height of the tower and of the spacers used to elevate it. Here are the different useful measurements for each lens-objective-stage configuration :
>
> | | **Height (mm)** | | | | |
> |---|---|---|---|---|---|
> | **Configuration** | **{Objective stage + adapter plate}** | **Objective spacer** | **Adapter plate** | **Optical axis** | **Tower spacers** |
> | 4-axis, no adapter plate | 30 | 18 | None | 80 | 5 |
> | 4-axis, 3D printed adapter plate | 30 | 22 | 5.70 | 84 | 9 |
> | 4-axis, aluminium adapter plate | 30 | 13 | 8.50 | 75 | 0 |

2. Then put the objective on the linear stage at the previously calculated height using the appropriate spacers ;
3. Align the objective with the beams coming from the lens so that those beams meet each other at the input of the objective (focal point of the lens) without reflecting on the metallic edges of the objective (both at the input and output of the objective).

> Note : If the beams are not meeting exactly at the height of the entrance point of the objective, then either the lens is not sufficiently well aligned, either the height of the objective is still not properly set.

6 Fine alignment of the lens using projection of the beams on a screen

Last check point :
Objective aligned.

6.1 Setting of the height of the lens

First, the beams must be made equidistant from the so-called "meeting point axis" (i.e. the axis on which the beams meets after the lens, which might not yet coincide perfectly with the proper-optical-axis). To do so, put a screen after the objective, with the objective out of focus, and adjust slightly the bottom screws of the 4-axis stage so that, when moving the objective out of focus along the propagation axis, both beams disappear on the screen at the same speed.

6.2 Setting of the tilt of the lens

Then, the tilt is set by putting the screen between the lens and the objective at a position such that the screen is not too close from the focal point in order to avoid the beams to be too close from each other - but also not too close from the lens, in order to avoid to be too close from the lens plane too.

6.3 Fine adjustment of the tilt of the lens

*To do **only** if the objective's entrance is exactly set at the height of the proper-optical-axis*

The tilt of the lens can then finely be tuned by putting a screen after the objective and observing how the beams move. To do so, one has to follow again the explanations detailed in 6.1 for setting the vertical position of the beams on the screen, but from now with the assumption that the beams positions are no longer relative positions as assumed in 6.1 (when taking as reference axis the meeting point axis) but are actually absolute positions (the meeting point axis is now assumed to coincide perfectly with the proper-optical-axis). Consequently, like in 6.1, one has to look at several different positions of the objective (so out of focus, notably at extinction positions of the beams) and make sure that both beams are always equidistant to their meeting point, as well as to make sure that the beams disappear at the same speed when going out of scope.

Notes :

- Actually, the aim of this step is to set the vertical position of the meeting point of the two beams on the proper-optical-axis. This is why only the position of the entrance of the objective matters (as it has previously been set at the height of the proper-optical-axis with spacers), and not the position of the exit of the objective (the 3D printed mount supporting the objective is not sufficiently stable for its parallelism with the ground to be reliable).
- Also, check the tilt of the lens putting the graduated rule between the PBS and the lens, looking at the two inner beams (which are retro-reflected ones) at the output of the rule ; those should be equidistant to the centre. If not, adjust one of the 4-axis stage bottom screws to change the tilt.
- If the beams are tilted on a screen placed after the objective, then it probably comes from the horizontal position of the lens. To correct that, adjust the top screws to translate the stage so that the incoming beams are well meeting on the vertical middle line of the lens.

7 Rough alignment of the camera and of the mirror leading to it

Last check point :
Lens finely aligned using projection of the beams on a screen.

1. Horizontal alignment :
   a) Use a graduated card and place it so that the middle line of the card is vertically aligned with the top screw of the camera (the screw located on the top face of the camera) ;
   b) Use this middle line to roughly align the beams horizontally with the camera.
2. Vertical alignment : turn on the camera to achieve fine alignment and then, on the software, activate the red circle and position it in the centre for guiding purpose. Use this red circle to vertically align the figure.

Notes : when roughly aligning the camera and the mirror leading to it (so before fixing the screws on the optical table), make sure that the retro reflected beams coming from the camera are well horizontally aligned with the objective (one can see those retro reflected beams at high intensity on the black plastic mount around the output of the objective), i.e. that those beams follow the same path as the incident beams. Then fix the screws on the optical table and adjust the alignment of the beams using the screws of the mirror.

8 Fine alignment of the camera and of the mirror leading to it

Last check point :
Camera and mirror leading to it roughly aligned.

- Place the beams at the centre of the camera adjusting the screws of the mirror leading to the camera and/or the position of the linear translation stage that supports the objective.

9 Adjustment of the intensity distribution

Last check point :
Camera and mirror leading to it finely aligned.

- Improve the intensity distribution between each beams by slightly rotating the bottom half-wave-plate located just before the bottom translation stage :

1. First by eye, using the intensity colour scale provided by the software and trying to have roughly the same amount of high-intensity-colour at the centre of each beam ;
2. Then with the measurement tools provided by the software :
   a) With the "TOTAL ISO" value provided by the LBP2 software for Newport beam profiler, or with the histogram tool provided by Spinview for the FLIR camera, blocking one beam then the other to compare and equalize their TOTAL ISO value or their maximum value ;
   b) With the intensity profiles that can be displayed on the left and on the bottom of the scope, trying to get peaks of same height for each beam.

10 Fine alignment of the lens with the camera

Last check point :
Intensity distribution adjusted and balanced between the two beams.

Preliminary notes :

- All along this step, one has to permanently know which beam coming out of the PBS corresponds to which beam observed with the camera, as the position of the beam coming from the top mirror (top beam before the lens) can easily be changed by slightly moving the screws of the top mirror, but the position of the beam coming from the back mirror (bottom beam before the lens) cannot. One has thus to check (when the objective is out of the focal point) whether the objective is located before or after the focal point, in order to figure out in which configuration the observed beams are.
  - If the objective is located before the focal point, the observed top (respectively bottom) beam corresponds to the top (respectively bottom) beam before the lens ;
  - On the contrary, if the objective is located after the focal point, then the observed top (respectively bottom) beam corresponds to the bottom (respectively top) beam before the lens.
- During this step, mainly the screws of the lens's stage need to be adjusted, although the top mirror screws may also need adjusting (at least the front one to horizontally better align the two beams) as well as the last mirror's screws (in order to relocate the beams on the camera when they are out of scope). The bottom screws of the lens's stage (that have not yet been properly set, and which control the vertical position of the beams) are used, and the top screws of the lens might also be (very cautiously though, as one has already set them previously).

Once the balance in intensity has been found, one can properly start the fine alignment of the lens. The idea is to achieve settings that are such that the interference pattern is present all the way along the translation stage motion with the same contrast. To do so, the beam separation is set to its minimum, and the position of the objective to the focal point. Then, the beam separation is increased and, playing with both the bottom left and bottom right screws of the lens's stage, the beams are brought closer to each other.

Note : It is important to note that the movements of these screws are not decorrelated (this correlation is minimized when the lens is placed on a corner of the stage). These screws must therefore be moved together to compensate for the movement of one of them by immediately moving the other screw in the appropriate direction.

Doing so for several different beam separation within its working range allows to reach the accordion configuration.

Sequence :

1. Proceed to the measurement of the position of the focal-point (i.e. the position of the objective's linear stage) and of the figure on the screen (relatively to the initial position of the figure) for several beam separations within the working range (complete measurement series).

   The idea is to estimate the current position of the focal-point and the orientation of the lens's optical axis relatively to the proper optical axis by quickly drawing the trend graphs for the current configuration of the lens.

   One can figure out if the lens's optical axis is bending or not relatively to the proper optical axis with the trend graphs of the horizontal and vertical positions of the figure. If it appears that the axis is bending, the amplitude and the direction in which it does can then be estimated, and the degree(s) of freedom that has/have to be set to correct can be identified.

2. Set the beam separation to the separation corresponding to the focal-point that is the furthest away from the estimated current-focal-point position according to the trend graphs ;
3. Then set the 4-axis stage (without changing the position of the objective) so that the beams move towards each other. This way, it brings the furthest position from the estimated convergence point closer to the latter position which is the estimated current-focal-point position ;

Notes :

- Those steps are tendency-dependent, that means that the trend graphs must regularly be updated, as well as the estimated current-focal-point position, in order to converge towards the perfect alignment configuration.

- If the lens looks too much tilted to the naked eye, then make it more vertical and proceed again from the beginning.
- Stop scanning the working range of beam separations as soon as the interference pattern is disappearing. Then set the lens keeping in mind that if big chnages of the screws must be achieved to improve the figure, then it is probably wrong for the whole range of positions, and so stop moving the screws before reaching the best figure in that case.

One can also proceed to the measurement of the position of the focal-point and of the figure on the screen for extreme beam separations only (quick measurement series) in order to get a quick idea of how the focal shift and the figure evolve with the new settings.
One can also try "by feel" going back and forth from one beam separation extrema to the other and slightly changing either the tilt or the vertical height of the lens between each step and checking if the alignment improved or not.

4. Once the settings can’t be improved anymore, proceed to a complete measurement series again in order to update the trend graph and to figure out the new tendency ;
5. Then repeat the whole process again and again until no further improvements are made.

Various other notes :

- While going back to the previous extreme position (so when you change the position of the bottom stage) if one notices that the beams get further away from each other and that they move (dramatically) on the horizontal axis, then the lens is probably horizontally misaligned, so one should then try (at the current intermediate position) to set the horizontal position of the lens so that beams overlap.
- If tilt is visible on the figure, then it is probably because of one of the three following reasons :

  1. If the fringes are tilted, this probably comes from an horizontal misalignment of the beams with respect to each other (i.e. an horizontal shift) ;
  2. If both beams are tilted in the same direction, this probably comes from the horizontal alignment of the lens ;
  3. If one beam is tilted relatively to the other one, this probably comes from the telescope settings ;

  Finally, note that some tilt can also come from the mirrors after the objective ; ideally, one should do the alignment directly after the objective, without mirror, but then the magnification is not good (too low).
- Better set the position of the objective to the focal position corresponding to the largest distance between the beams so that, when reducing the distance between the beams, even if the focal point move, partial overlapping of the beams still occurs. Otherwise, beams will probably go out of scope for large beam separations.
- The position of the figure on the scope of the software is more related to the tilt than to the position.
- Record the position with the centroid parameters in the software.
- To improve the horizontal alignment, look at the orientation showed by the software for each beam (blocking one beam) and try to make this orientation as close as possible from 0° by changing the settings of horizontal position and tilt.

Appendix B : Fourier transform of the intensity

Starting from the expression of the vertical cross-section of the figure :

$$I(y) = A\left[1 + C \cdot \underbrace{\cos\left(2\pi\frac{y}{d} + \Phi\right)}_{\equiv h(y)}\right] \cdot \underbrace{\exp\left[-2\left(\frac{y - y_0}{w_y}\right)^2\right]}_{\equiv g(y)}, \tag{1}$$

where the constant term B has been neglected so as not to have to handle the Fourier transform of a constant throughout the calculation, one can write :

$$FT[I(y)] = A \cdot FT[g(y)] + A \cdot C \cdot FT[h(y) \cdot g(y)] \tag{2}$$

Now, on the one hand :

$$\begin{aligned} FT[g(y)] &= \int_{-\infty}^{+\infty} g(y) e^{-i2\pi f y} dy \\ &= \int_{-\infty}^{+\infty} \exp\left[-2\left(\frac{y - y_0}{w_y}\right)^2\right] e^{-i2\pi f y} dy \end{aligned} \tag{3}$$

In other words, with the change of variable $u = y - y_0$:

$$\begin{aligned} FT[g(y)] &= \int_{-\infty}^{+\infty} \exp\left[-\frac{2}{w_y^2} \cdot u^2\right] \exp\left[-i2\pi f\,(u + y_0)\right] du \\ &= e^{-i2\pi f y_0} \cdot \int_{-\infty}^{+\infty} \exp\left[-\frac{2}{w_y^2} \cdot u^2\right] \cdot e^{-i2\pi f u} du \end{aligned} \tag{4}$$

Where the Fourier transform of a Gaussian function is identified :

$$\int_{-\infty}^{+\infty} e^{-\alpha u^2} \cdot e^{-i2\pi f u} du = \sqrt{\frac{\pi}{\alpha}} \cdot \exp\left[-\frac{\pi^2}{\alpha} \cdot f^2\right], \quad \text{with } \alpha \equiv \tfrac{2}{w_y^2}.$$

$$\text{So} : FT[g(y)] = \widetilde{G}(f) = \sqrt{\frac{\pi}{2}} \cdot w_y \cdot \exp\left[-\frac{\pi^2 w_y^2}{2} \cdot f^2 - i2\pi y_0 \cdot f\right] \tag{5}$$

On the other hand :

$$\begin{aligned} h(y)\cdot g(y) &= \cos\left(2\pi\frac{y}{d}+\Phi\right) g(y) \\ &= \left[\cos\left(2\pi\frac{y}{d}\right)\cos(\Phi) - \sin\left(2\pi\frac{y}{d}\right)\sin(\Phi)\right] g(y) \\ &= \cos(\Phi)\left[\cos\left(2\pi\frac{y}{d}\right) g(y)\right] - \sin(\Phi)\left[\sin\left(2\pi\frac{y}{d}\right) g(y)\right] \end{aligned} \tag{6}$$

Therefore, with $\begin{cases} FT\left[\cos\left(2\pi\frac{y}{d}\right)\right] = \frac{\delta\left(f-\frac{1}{d}\right)+\delta\left(f+\frac{1}{d}\right)}{2} \\ FT\left[\sin\left(2\pi\frac{y}{d}\right)\right] = \frac{\delta\left(f-\frac{1}{d}\right)-\delta\left(f+\frac{1}{d}\right)}{2i} \end{cases}$:

$$\begin{aligned} FT[h(y)\cdot g(y)] &= \frac{1}{2}\cos(\Phi)\left[\widetilde{G}\left(f-\frac{1}{d}\right)+\widetilde{G}\left(f+\frac{1}{d}\right)\right] - \frac{1}{2i}\sin(\Phi)\left[\widetilde{G}\left(f-\frac{1}{d}\right)-\widetilde{G}\left(f+\frac{1}{d}\right)\right] \\ &= \frac{1}{2}[\cos(\Phi)+i\sin(\Phi)]\widetilde{G}\left(f-\frac{1}{d}\right) + \frac{1}{2}[\cos(\Phi)+i\sin(-\Phi)]\widetilde{G}\left(f+\frac{1}{d}\right) \\ &= \frac{1}{2}e^{i\Phi}\widetilde{G}\left(f-\frac{1}{d}\right) + \frac{1}{2}e^{-i\Phi}\cdot\widetilde{G}\left(f+\frac{1}{d}\right) \end{aligned} \tag{7}$$

In other words :

$$\begin{aligned} FT[h(y)\cdot g(y)] = \widetilde{HG}(f) = \frac{1}{2}\sqrt{\frac{\pi}{2}}\cdot w_y \Bigg\{ &\exp\left[-\frac{\pi^2 w_y^2}{2}\left(f-\frac{1}{d}\right)^2 - i2\pi y_0(f-d) + i\Phi\right] \\ &+ \exp\left[-\frac{\pi^2 w_y^2}{2}\left(f+\frac{1}{d}\right)^2 - i2\pi y_0(f+d) - i\Phi\right]\Bigg\} \end{aligned} \tag{8}$$

So the Fourier transform $\widetilde{I}$ of the vertical cross-section of the interference pattern writes:

$$\begin{aligned} \widetilde{I}(f) \;&= A\sqrt{\frac{\pi}{2}}\cdot w_y\cdot\exp\left[-\frac{\pi^2 w_y^2}{2}f^2 - i2\pi y_0 f\right] \\ &+ \frac{A\cdot C}{2}\cdot\sqrt{\frac{\pi}{2}}\cdot w_y\cdot\Bigg\{\exp\left[\frac{-\pi^2 w_y^2}{2}\left(f-\frac{1}{d}\right)^2 - i2\pi y_0\left(f-\frac{1}{d}\right) + i\Phi\right] \\ &+ \exp\left[\frac{-\pi^2 w_y^2}{2}\left(f+\frac{1}{d}\right)^2 - i2\pi y_0\left(f+\frac{1}{d}\right) - i\Phi\right]\Bigg\} \end{aligned} \tag{9}$$

Alphabetical Index

Résumé

Les expériences de gaz quantiques constituent une plateforme incontournable pour l'étude des phénomènes quantiques à N corps, permettant la simulation de problèmes de physique de la matière condensée autrement inaccessibles. Bien que pendant de nombreuses années, la plupart des expériences de gaz quantiques aient été consacrées à des atomes alcalins tels que le rubidium ou le sodium, la dernière décennie a marqué un tournant sur le plan de la physique avec la réalisation de condensats de Bose-Einstein d'atomes de la famille des lanthanides, tels que le dysprosium. Ces nouvelles expériences, mettant à profit le grand moment magnétique des lanthanides, ont considérablement élargi l'éventail des problèmes de physique accessibles expérimentalement, ajoutant des interactions anisotropes et à longue portée aux interactions à courte portée déjà exploitées avec les atomes alcalins.

C'est dans ce contexte que s'est déroulé le stage dont il est question dans ce rapport. Effectué au sein du groupe Quantum Fluids du Prof. Dr. Lauriane Chomaz au Physikalisches Institut de Heidelberg en Allemagne, ce stage avait pour but de contribuer à une expérience d'atomes froids de dysprosium conçue pour étudier les propriétés physiques des gaz quantiques dipolaires en dimensions réduites et les phénomènes qui se produisent dans de tels systèmes physiques (gouttelettes quantiques, supersolidité, superfluidité).

Cette expérience, actuellement en cours de construction, implique la production et l'étude d'un gaz quantique d'atomes de dysprosium d'isotope bosonique ^{164}Dy amenés dans la phase de condensat de Bose-Einstein et réduits à deux dimensions. Il nécessite la mise en place d'un système de confinement poussé de ce condensat par compression le long d'une direction : le réseau en accordéon, système au centre du travail de stage rapporté dans le présent document.

Mots-clé

Physique atomique, moléculaire, et optique, gaz quantiques dipolaires, réseau en accordéon, physique expérimentale, dysprosium, Quantum Fluids Heidelberg.

Abstract

Quantum gases experiments constitute a paradigmatic platform for the investigation of many-body quantum phenomena, enabling simulation of otherwise inaccessible condensed matter physics problems. Although for many years most of the quantum gases experiments were dealing with alkali atoms like rubidium or sodium, the last decade marked a turning point on the physical point of view with the achievement of Bose-Einstein condensates of lanthanide atoms like dysprosium. These new experiments, taking advantage of the large magnetic moment of lanthanides, expanded considerably the range of experimentally accessible physics problems, adding long-range and anisotropic interactions to the already exploited short-range interactions of alkali atoms.

It is in this context that the internship discussed in this report took place. Performed in Prof. Dr. Lauriane Chomaz's Quantum Fluids group at the Physikalisches Institut of Heidelberg in Germany, this internship aimed at contributing to a cold atom experiment of dysprosium designed to study the physical properties of dipolar quantum gases in reduced dimensions and the phenomena occurring in such physical systems, like the emergence of exotic phases of quantum matter (quantum droplets, supersolid, superfluid).

This experiment, currently under construction, involves the production and study of a quantum gas of ^{164}Dy bosonic dysprosium atoms brought into the phase of a Bose-Einstein condensate and reduced to two dimensions. It involves setting up a system for cooling atoms below the critical temperature of the phase transition between a thermal gas and a Bose-Einstein condensate, as well as a system for tightly confining this condensate by compression along one direction : the accordion lattice.

The aim of this report is to describe some of the main ideas underlying such an experiment, through the description of the work achieved during an internship on the accordion lattice test setup of the Quantum Fluids group at the Physikalisches Institut Heidelberg.

Key-words

Atomic, molecular, and optical physics, dipolar quantum gases, accordion lattice, experimental physics, dysprosium, Quantum Fluids Heidelberg.